Published in final edited form as:

Nature. 2021 August ; 596(7870): 138–142. doi:10.1038/s41586-021-03764-0.

Structural basis of human separase regulation by securin and Cdk1-cyclin B1

Jun Yu[1], **Pierre Raia**[1,*], **Chloe M. Ghent**[2,*], **Tobias Raisch**[3,*], **Yashar Sadian**[4], **Simone Cavadini**[5], **Pramod M. Sabale**[6], **David Barford**[7], **Stefan Raunser**[3], **David O. Morgan**[2], **Andreas Boland**[1]

[1]Department of Molecular Biology, University of Geneva, CH-1211 Geneva, Switzerland

[2]Department of Physiology, University of California, San Francisco, San Francisco, CA 94143, USA

[3]Department of Structural Biochemistry, Max Planck Institute of Molecular Physiology, 44227 Dortmund, Germany

[4]Bioimaging Center, University of Geneva, CH-1211 Geneva, Switzerland

[5]Friedrich Miescher Institute for Biomedical Research, CH-4058 Basel, Switzerland

[6]Department of Organic Chemistry, NCCR Chemical Biology, University of Geneva, CH-1211 Geneva, Switzerland

[7]MRC Laboratory of Molecular Biology, Cambridge, CB2 0QH, UK

Abstract

In early mitosis, the duplicated chromosomes are held together by the ring-shaped cohesin complex[1]. Chromosome separation in anaphase is triggered by separase, a large cysteine endopeptidase that cleaves the cohesin subunit Scc1/Rad21[2–4]. Separase is activated by degradation of its inhibitors securin[5] and cyclin B[6], but the molecular mechanisms of separase regulation are not clear. Here, we used cryogenic electron microscopy (cryoEM) to determine the structures of human separase in complex with either securin or Cdk1-cyclin B1-Cks1. In both complexes, separase is inhibited by pseudosubstrate motifs that block substrate binding at the active site and at nearby docking sites. As in *Caenorhabditis elegans*[7] and yeast[8], human securin harbors its own pseudosubstrate motifs. In contrast, Cdk1-cyclin B1 inhibits separase by deploying pseudosubstrate motifs from intrinsically disordered loops in separase itself. One autoinhibitory loop is oriented by Cdk1-cyclin B1 to block the active sites of both separase and

Corresponding Author and Lead Contact: Andreas Boland (Andreas.Boland@unige.ch), **Contact information**, Department of Molecular Biology, University of Geneva, Geneva, Switzerland.

*these authors contributed equally.

Author Contributions Statement

J.Y. expressed and purified the securin$^{\Delta 160}$-separase complexes, the MBP-securin fusions and the Cdk1-cyclin B1-Cks1 complexes. C.M.G. purified securin$^{\Delta 138}$-separase fusion protein. P.R. and C.M.G. performed separase cleavage activity assays. J.Y. and Y.S. prepared grids and T.R. collected EM data with contributions from S.C. and A.B. J.Y. and P.R. analyzed EM data and J.Y. determined the 3D reconstructions. J.Y. and Y.S. built the model *ab initio* and P.R. made the figures. A.B. directed the project and designed experiments together with D.O.M. A.B. and D.O.M. wrote the manuscript with contributions and discussions from J.Y., P.R., C.M.G., T.R., Y.S., P.M.S., D.B. and S.R.

Competing Interests Statement

The authors declare no competing interests.

Cdk1[9,10]. Another autoinhibitory loop blocks substrate docking in a cleft adjacent to the separase catalytic site. A third separase loop contains a phosphoserine[6] that promotes complex assembly by binding to a conserved phosphate-binding pocket in cyclin B1. Our study reveals the diverse array of mechanisms by which securin and Cdk1-cyclin B1 bind and inhibit separase, providing the molecular basis for the robust control of chromosome segregation.

Accurate and timely chromosome segregation is critical for genomic stability and to prevent aneuploidy and tumorigenesis[11,12]. Cohesin cleavage is therefore tightly regulated prior to anaphase by mutually exclusive binding of separase to either its inhibitory chaperone securin[2,12–14] or a heterodimeric complex of Cdk1 and cyclin B1[6,10] or cyclin B2[15]. Separase is also inhibited by shugoshin-Mad2 during a spindle checkpoint arrest[16]. Phosphorylation of separase serine 1126 by Cdk1 is essential for cyclin B1-separase binding[6] and enables Pin1-dependent cis/trans isomerization of proline 1127, which might be required for cyclin B1 binding *in vivo*[17]. Ubiquitin-mediated destruction of securin and cyclin B1 unleashes separase in late metaphase. Some separase remains associated with a subset of cyclin B1-Cdk1 and inhibits Cdk1 activity[9,10], allowing normal anaphase chromosome movement[18].

Structures of fungal and *C. elegans* separase, in complex with a substrate mimic or securin, revealed some of the molecular features of substrate recognition[19] and inhibition by securin[7,8]. Securin contains a conserved sequence motif, EIExxΦ (referred to as positions P6-P1), that resembles the minimal consensus cleavage site in separase substrates ([D/E/S]xExxR)[20]. Substitution of the arginine residue at P1 with a hydrophobic residue distorts the catalytic site and prevents substrate cleavage[7,8,21]. A basic groove on separase, at the P6 substrate position, explains enhanced Scc1 cleavage upon phosphorylation of a P6 serine[19,22]. Substrates also interact with separase outside its catalytic site: Scc1 contains a separase-binding motif (LPE), distant from the cleavage site, that promotes separase cleavage[13]. Securin contains a related motif, suggesting that it acts in part by blocking substrate docking. However, the molecular mechanisms of separase regulation remain poorly understood.

Architecture of human separase complexes

To better understand inhibition of human separase by securin and the Cdk1-cyclin B1-Cks1 (CCC) complex, we used cryoEM to determine the structures of the human separase-securin and separase-CCC complexes.

Whereas human separase-securin complex is readily prepared in large quantities[7] (Extended Data Fig. 1a), reconstitution of the separase-CCC complex required the fusion of a short C-terminal segment of securin to the N-terminal HEAT-repeat domain of separase[13] (Extended Data Fig. 1a). We included the phosphothreonine-binding subunit Cks1 because it is an integral part of the Cdk1-cyclin complex[6,23] and confers specificity for phosphorylated substrates[24,25]. We found that stable CCC association with separase *in vitro* is ATP-dependent, consistent with a role for separase phosphorylation (Extended Data Fig. 2a, b). Mass spectrometry analysis of these preparations showed phosphorylation at Ser1126

(Extended Data Fig. 2c, d). Pin1-mediated cis/trans isomerization of proline 1127 was not required for complex assembly (Extended Data Fig. 2a, b).

We determined the structures of a wild-type separase-securin complex and a catalytically-inactive securin$^{\Delta 160}$-separase^{C2029S}-CCC complex, at overall resolutions of ~2.9 Å and ~3.6 Å, respectively (Fig. 1, Extended Data Fig. 1b–e; Extended Data Table 1, Supplementary Video 1). We also imaged a securin$^{\Delta 138}$-separase^{C2029S} fusion protein, which displayed an overall conformation very similar to that of the separase-securin complex (Extended Data Fig. 1b, c)[13].

Human separase consists of an N-terminal HEAT-repeat domain (residues 1-666) followed by a large TPR-like domain (residues 667-1706) and a C-terminal protease domain (residues 1707-2120). The TPR-like domain is interrupted by two intrinsically disordered inserts (insert 1, residues 1065–1152; insert 2, residues 1278–1572) (Fig. 1a) that are important for separase regulation[4,6,23,26,27]. This overall architecture is shared with most other known separase proteases[28], except that the diverse N-terminal domain has been lost in some organisms such as *C. elegans*[7,29].

The EM maps provide excellent side chain density in the TPR-like and C-terminal protease domains (Extended Data Fig. 3), whereas the N-terminal domain is less well-defined due to its inherent flexibility (Fig. 1b, c, Extended Data Figs. 1c, 4, 5). Focused refinement with partial signal subtraction slightly improved the resolution of the TPR-like and protease domains (Extended Data Fig. 1d). Density for the N-terminal ~250 residues can be observed in the EM map at very low thresholds and a putative full-length separase model is shown in Extended Data Fig. 6c. Binding of full-length securin across all three domains of separase seems to reduce the flexibility of the N-terminus, as suggested by the almost complete absence of density for the N-terminal regions when separase is bound to CCC (Fig. 1c, Extended Data Figs. 1e, 5). The HEAT-repeat domain adopts an extended rod-shaped conformation with ~90 Å in its longest dimension. The yeast N-terminal domain adopts a much more compact fold, with the N-terminus of the yeast protein folding back in close proximity to the TPR-like domain (Extended Data Fig. 6a, b)[8].

Separase inhibition by pseudosubstrate motifs

Separase inhibition in both complexes depends on conserved substrate-mimicking sequences that block substrate binding at the separase catalytic site and at nearby docking sites. In the separase-securin complex, these pseudosubstrate motifs are present in securin. In the separase-CCC complex, however, these motifs are found in loops of separase itself. Upon binding of CCC, three autoinhibitory loops (AILs) undergo a disorder-to-order transition and bind to various sites on separase and the CCC complex (Fig. 2a–e, Extended Data Fig. 7, Supplementary Video 2). One of these loops, AIL3, lies within the large insert 2 (Fig. 1a).

The EIExxΦ pseudosubstrate motif in securin (or [D/E/S]xExxR in Scc1[20]) binds the catalytic site of separase similarly to a substrate-mimic peptide fused to the separase protease domain from *Chaetomium thermophilum*[19] (Fig. 2a–c). In the separase-CCC complex, AIL3 of separase mimics these interactions. AIL3 harbors an NFS sequence

(residues 1394-1396) that, when compared to securin and Scc1, binds to separase in an inverse orientation, with Ser1396 and Asn1394 binding to the P6 and P4 positions, respectively. Phe1395 (P5) of separase forms hydrophobic stacking interactions with Trp1776^{Sep} as observed for Scc1 and securin (Fig. 2c). C-terminal acidic sequences in AIL3 are recognized by the basic groove in separase, comparable to phosphorylated Scc1 in yeast[19] (Fig. 2c, Extended Data Figs. 7a, 8). Phosphorylation of Ser1396 and Ser1399 has been detected in mitotic cells[23,30] and our structure suggests this might promote AIL3 binding.

A second motif, NxLxΦE, forms a small α-helical structure in a cleft between the TPR-like domain and the protease domain in both complexes (Fig. 2a, b, d). This motif is present in securin (NPLDFE; residues 121-126) and in a loop (AIL1) of separase (NDLNYE; residues 715-720). In separase, Phe712 (three amino acids N-terminal of NDLNYE) might correspond to the P1 residue in securin (Phe118) by directly interacting with and displacing the catalytic histidine (His2003) (Fig. 2d, Extended Data Fig. 7b). Interestingly, a similar motif is found in the substrate Scc1 (NHLEYE; residues 207-212) between the cleavage site (DREIMR; residues 167-172) and a substrate docking motif (LPE; residues 254-256)[13]. We analyzed separase-mediated cleavage of Scc1 with deletions in this region, revealing that efficient cleavage requires the segment containing the NHLEYE motif (Extended Data Fig. 9a). Glu210 and Tyr211 are critical residues (Fig. 2f, Extended Data Fig. 9b). Thus, the Scc1 NHLEYE motif promotes Scc1 binding to separase, and securin and the CCC complex block this interaction.

30-40-residue linkers separate the Scc1 cleavage site and the two substrate-docking motifs. Deletion of these linkers, or replacement with a random sequence, abolished Scc1 cleavage *in vitro*, indicating that these sequences also contribute to Scc1 binding (Extended Data Fig. 9c).

The LPE docking motif of Scc1 also exists in securin (residues 130-132)[13]. In the separase-securin complex, this motif interacts with a hydrophobic pocket formed by Ala1009 and Phe1010 and a basic surface formed by Lys944 and Arg947 (Fig. 2e, Extended Data Fig. 7c). The LPE-binding site is unoccupied in the separase-CCC complex.

We tested the function of the autoinhibitory loops AIL1 and AIL3 by analysis of separase mutants with deletions in one or both loops (Extended Data Table 2, Extended Data Fig. 10d). Deletion of the pseudosubstrate motifs in AIL1 or AIL3 resulted in increased Scc1 cleavage rates, suggesting that these motifs have some inhibitory effect even in the absence of the CCC complex (Fig. 2g, Extended Data Fig. 10a). As expected, these deletions displayed resistance to inhibition by the CCC complex (Extended Data Fig. 10b), due in part to lower affinity for the complex (Extended Data Fig. 10c).

A stretch of hydrophobic residues C-terminal of the LPE motif (residues 136-146) mediates the insertion of securin into a hydrophobic channel of separase. In the separase-CCC complex, a short separase loop, AIL2, inserts into this channel (Extended Data Figs. 7d, 11a). Studies of truncated securin mutants revealed that this hydrophobic stretch is required for high-affinity securin-separase binding and inhibition of separase activity (Extended Data

Fig. 11b–d). We propose that occupation of the hydrophobic channel by securin or AIL2 reduces Scc1 binding.

Separase binding to Cdk1-cyclin B1

The CCC complex binds at the periphery of the TPR-like domain and the C-terminal protease domain, thereby bridging a clearly defined cleft between the domains. As a result, the intrinsically disordered insert 1 in separase (Fig. 1a) becomes structured and wraps around cyclin B1, providing a binding platform through mainly nonspecific main chain-main chain interactions (Figs. 1c, 3a, Extended Data Fig. 12). This cyclin B1-binding loop contains phosphorylated serine 1126 at its center, and density for the phosphate group is clearly visible in our EM map (Fig. 3a, Extended Data Fig. 3e, Supplementary Video 3). This loop also interacts with the substrate-docking hydrophobic patch of cyclin B1 through a binding motif (residues 1100-1102) that is inverted when compared to common cyclin B1-binding partners (Fig. 3a, Extended Data Fig. 13a).

Phosphoserine 1126 engages a previously unidentified phosphate-binding pocket in cyclin B1 (Figs. 1a, 3a). Three conserved amino acids (Arg307, His320 and Lys324) form a hydrogen-bonding network with the phosphate group (Fig. 3a, Extended Data Fig. 13c). Lys408 and His409 of cyclin B1 might also contribute to phosphoserine recognition. Surface charge analysis reveals a positively-charged binding pocket in cyclin B1 but not in cyclin A (PDB code: 1JSU[31]) (Extended Data Fig. 13).

The structure of Cdk1 in the separase-CCC complex superimposes well with an activated Cdk2-cyclin A-substrate peptide complex (PDB code: 2CCI[32]). The conserved DFG motif of the kinase catalytic site is in its inwards conformation, Thr161 is phosphorylated and the activation loop adopts an active conformation (Fig. 3b, Extended Data Fig. 14a). The glycine-rich loop (residues 11-16) is in a downwards conformation relative to Cdk2 bound to ATP, sterically precluding ATP binding. Additionally, EM density can be observed around Thr14, potentially due to its phosphorylation.

AIL3 of separase contains a Cdc6-like domain that binds and inhibits Cdk1-cyclin B1[10,23]. Residues Pro1375 to Arg1386 interact with the substrate-binding site of Cdk1. Most importantly, the conserved APxxxxR motif[10] serves as a pseudosubstrate that resembles the consensus Cdk phosphorylation site (SPxR), except that the phosphoacceptor serine is replaced with an alanine (Ala1380) and Arg1386 reaches back to mimic the basic side chain that is usually found at P+3 of Cdk substrates (Fig. 3b, Supplementary Video 3). Trp168 of Cdk1 serves as an electron-stacking partner for Val1377 N-terminal of the APxxxxR motif. The pseudosubstrate motif superimposes well with an ideal substrate peptide co-crystallized with Cdk2-cyclin A[32] (Fig. 3b). Just C-terminal of the APxxxxR motif, the loop contacts cyclin B1 through amino acids 1386-1391 (particularly Val1387, Thr1389, Arg1390 and Leu1391), completing the series of interactions that promote binding and inhibit Cdk1 activity (Extended Data Fig. 14b, c).

Cks1 does not directly contact any rigid structure elements of separase (Fig. 1c). However, we observe strong density around the phosphate-binding pocket of Cks1, suggesting

that a separase phosphorylation site is occupying this site (Extended Data Fig. 3f). Phosphorylation of AIL3 is known to promote Cdk-cyclin binding, and Thr1346 has been proposed as a key phosphorylation site[6,10]. Cks1 has a preference for phosphothreonine-proline sequences[25]. Thr1346 lies in a disordered region that is not visible in our structure; it is therefore plausible that this site occupies Cks1.

Discussion

Consistent with previous studies, we find that securin acts as an extended pseudosubstrate that blocks substrate binding at the catalytic site and at nearby docking sites. Unexpectedly, Cdk1-cyclin B1-Cks1 suppresses separase activity by activating autoinhibitory sequences in loops of separase itself (Fig. 2a–e, Extended Data Fig. 6a).

Detailed comparison of separase sequences from multiple species[33] reveals that the docking sequence in AIL1 is well conserved only in vertebrates and has co-evolved with the presence of the cyclin B-binding loop and the Cdc6-like domain, suggesting that regulation of separase activity by the CCC complex might be specific for vertebrates.

Separase is also inhibited by the shugoshin 2 (Sgo2)-Mad2 complex during activation of the spindle assembly checkpoint[16]. Sgo2 contains a pseudosubstrate motif that is thought to mediate inhibition at the active site[16]. Sgo2 and Mad2 also contain LPE-related motifs that could inhibit substrate docking, but detailed structural analysis will be required to determine the precise mode of separase inhibition.

We identify for the first time a phosphate-binding pocket in cyclin B1. The key residues of this pocket are conserved in B- but not A-type cyclins (Fig. 3a, Extended Data Fig. 13c), explaining the specificity of cyclin B1 and B2 for separase binding. We suspect that this phosphate-binding pocket is employed by B-type cyclins to mediate interactions with phosphorylated regulators or substrates. Indeed, mutations in this region are known to inhibit interactions with the phosphatase Cdc25C, a key Cdk1 regulator[34]. It seems likely that this phosphate-binding site, like the phosphate-binding site of Cks1, also enhances binding and modification of specific pre-phosphorylated Cdk1 substrates[24].

We propose that binding of Cdk1-cyclin B1 to separase occurs in a series of distinct steps. First, Cdk1-cyclin B phosphorylates separase at Ser1126 and other sites, such as Thr1346[6,10]. Phosphoserine 1126 then interacts with the phosphate-binding pocket on the same or another cyclin B1 to initiate complex formation, causing insert 1 to surround cyclin B1 and interact with Cdk1 (Figs. 2a, 3a, b, Extended Data Fig. 12). Binding of cyclin B1 to the TPR-like domain stabilizes insertion of the separase NDLNYE motif of AIL1 in the cleft next to the catalytic site. Finally, the pseudosubstrate motifs of AIL3 bind to the active sites of Cdk1 and separase.

Three separase-binding motifs (EIExxΦ, NPLDFE, LPE) are immediately adjacent to each another in the securin sequence, and bind to three closely-spaced binding sites on separase. In human Scc1, however, the three equivalent motifs are separated by long intervening sequences that are also required for rapid Scc1 cleavage (Extended Data Fig.

9c). Simultaneous binding of all three motifs to separase would require looping out of the intervening spacer regions.

Taken together, our results reveal the complex array of mechanisms by which separase and Cdk1-cyclin B bind and inhibit each other, and provide a striking example of the power of short linear pseudosubstrate motifs in enzyme regulation.

Material and Methods

Cloning

The cDNAs encoding human proteins (separase, securin, Pin1, Cdk1, cyclin B1 and Cks1) were ordered as gene optimized versions for expression in *Spodoptera frugiperda* (Sf9) cells. Synthesized cDNA (Thermo Fisher Scientific) of separase (1-2120) and securin (1-202) together with a dual promoter were subcloned into a pF1 vector[35] with a Twin-StrepII tag followed by a TEV site at the C-terminus of securin. Separase-securin fusion constructs were made by fusing a securin fragment (160-202) or the full-length sequence to the N-terminus of separase with a GS-linker and a TEV site in between[13]. Securin fragments (residues 1-127, 1-138, 1-157 and 1-202) and full length Pin1 were cloned into the pETM41 vector with a His-MBP tag at the N-terminus for BL21 (DE3) *E. coli* expression. The human Polo Kinase Plk1 (residues 37-338) construct was kindly provided by Claudio Alfieri (ICR, London). Cdk1, cyclin B1 and Cks1 were cloned into the pF1 vector for co-expression according to Zhang *et al.*[35]. A Twin-StrepII tag and an 8×His tag were fused to the C-terminus of Cdk1 and cyclin B1, respectively. All deletions and mutations were generated by mutagenesis PCR.

Purification of separase complexes

Human separase constructs, as well as the Cdk1-cyclin B1-Cks1 complex, were expressed in Sf9 cells using baculoviruses. Typically, 25 ml of recombinant P3 baculoviruses were used to infect 500 ml of Sf9 insect cells (Invitrogen) at a cell density of roughly $2.0x10^6$ cells per ml. The cells were incubated for 48 hours at 27 °C at 110 rev/min, harvested at a cell viability rate of 80-85%, flash-frozen in liquid nitrogen and stored at −80 °C. Securin constructs (residues 1-127, 1-138, 1-157 and 1-202), full length Pin1 and Plk1 (residues 37-338) were expressed in BL21 (DE3) *E. coli* at 18 °C for 16 h after induction with IPTG (Isopropyl β-d-1-thiogalactopyranoside).

Purification of all proteins and protein complexes was performed at 4 °C. Cells expressing human separase-securin were resuspended in lysis buffer (50 mM HEPES-KOH pH 7.8, 300 mM KCl, 5% glycerol, 0.5 mM EDTA, 0.5 mM TCEP) containing protease inhibitor cocktail tablets (PIC) (Complete EDTA-free; Roche Diagnostics GmbH), and 5 units/ml supernuclease (Novagen), subsequently sonicated and centrifuged for 1 h at 40,000 g. The soluble fraction was slowly (0.8 ml/min flow rate) applied onto a 5 ml StrepTactin Superflow Cartridge (Qiagen) and the column was washed with high-salt buffer (50 mM HEPES-KOH pH 7.8, 900 mM KCl, 5% glycerol, 0.5 mM EDTA, 0.5 mM TCEP) until stable UV absorption was observed. Proteins were eluted in wash buffer containing 2.5 mM desthiobiotin. A final size exclusion step on a Superose 6 Increase 10/300 GL column

(GE Healthcare Life Sciences) pre-equilibrated in 20 mM HEPES-KOH pH 7.8, 100 mM KCl, 10 mM $MgCl_2$ and 0.5 mM TCEP was performed. The purified proteins were pooled, concentrated, flash-frozen and stored at −80 °C.

The Cdk1-cyclin B1-Cks1 complex was purified using StrepTactin Superflow Cartridge (Qiagen) columns. Lysis and wash buffer contained 50 mM Tris-HCl pH 8.0, 500 mM NaCl, 10 mM β-mercaptoethanol and 5% glycerol. The complex was eluted using wash buffer supplemented with 2.5 mM desthiobiotin and further loaded onto a HisTrap HP column (GE Healthcare Life Sciences). To elute protein complexes, we used 50 mM Tris-HCl pH 8.0, 500 mM NaCl, 250 mM imidazole, 10 mM β-mercaptoethanol and 5% glycerol. Peak fractions were pooled, concentrated and loaded on a Superose 6 Increase 10/300 GL column (GE Healthcare Life Sciences) size exclusion column as a final purification step.

Different lengths of securin (residues 1-127, 1-138, 1-157 and 1-202) and Plk1 were purified as described by Zhang *et al.*[36]. Briefly, proteins were purified using a HisTrap HP column (GE Healthcare Life Sciences) in 50 mM Tris-HCl pH 7.5, 300 mM NaCl, 20 mM imidazole, 10 mM β-mercaptoethanol and 5% glycerol lysis buffer and 50 mM Tris-HCl pH 7.5, 1 M NaCl, 20 mM imidazole, 10 mM β-mercaptoethanol and 5% glycerol high-salt buffer and subsequently eluted by an imidazole gradient. Securin proteins were loaded onto a Superdex 200 Increase 10/300 GL gel filtration column (20 mM HEPES-NaOH pH 7.5, 100 mM NaCl and 0.5 mM TCEP).

Plk1 was purified using a His-tag, treated with TEV protease at 4 °C overnight and the tag was removed by re-binding to a HisTrap HP column. A final size exclusion step using a Superdex 75 Increase 10/300 GL column was performed.

Pin1 was purified over an MBPTrap HP column (GE Healthcare Life Sciences). We used 50 mM Tris-HCl pH 7.5, 300 mM NaCl, 2mM DTT and 5% glycerol as lysis and wash buffer. The proteins were eluted by adding 10 mM maltose, followed by TEV cleavage at 4 °C overnight. The sample was further purified by a HisTrap HP column and gel filtration in 20 mM HEPES-NaOH pH 7.5, 100 mM NaCl and 0.5 mM TCEP.

Assembly of securin$^{\Delta 160}$-separase^{C2029S}-Cdk1-cyclin B1-Cks1 complex

Purified securin$^{\Delta 160}$-separase^{C2029S} fusion protein was mixed with Cdk1-cyclin B1-Cks1 complexes in a molar ratio of 1:1.5 in a reaction buffer of 50 mM HEPES pH 8.0, 100 mM NaCl, 10 mM $MgCl_2$, 5 mM ATP and 0.5 mM TCEP. The reaction mixture was incubated at room temperature for 40 min followed by gel filtration on a Superose 6 3.2/300 column (GE Healthcare Life Sciences) in 20 mM HEPES pH 8.0, 150 mM NaCl, 5 mM $MgCl_2$ and 0.5 mM TCEP. Fractions containing securin$^{\Delta 160}$-separase^{C2029S}-Cdk1-cyclin B1-Cks1 complexes were pooled and concentrated.

Separase cleavage assays

For studies of the NHLEYE and LPE motifs of Scc1, ^{35}S-methionine-labeled human Scc1 (residues 142-300) was produced in rabbit reticulocyte lysates and purified as described previously[13]. Deletion and point mutations were constructed by Gibson cloning. Purified securin$^{\Delta 138}$-separase fusion protein[13] (0.14 μM final concentration) was mixed 1:1 with

purified Scc1 substrate and incubated for 30 min at 25 °C. Reaction products were analyzed by SDS-PAGE and visualized with a Phosphorimager.

To dissect the effect of mutations on the separase auto-inhibitory loop segments, ^{35}S-methionine-labeled human full-length Scc1 was produced using wheat germ extract systems (Promega) and 0.8 μCi/μl of ^{35}S-methionine was added. Following *in vitro* translation, Scc1 was phosphorylated by adding 4 μM polo-like kinase (Plk1), 5 mM ATP, 10 mM $MgCl_2$ and incubated for 2 h at 30 °C. 1.5 μM of human separase was mixed with 10x molar excess of human securin. The cleavage reaction was stopped after 20 min at 30 °C. Reaction products were analyzed by SDS-PAGE with BioRad 4–20% TXP gels and visualized with a Phosphorimager.

Pull-down assays

Purified securin proteins (N-terminal His-MBP tag) were mixed with securin$^{\Delta 160}$-separase^{C2029S} and incubated with 40 μL amylose beads for 1 hour at 4 °C (50 mM HEPES pH 8.0, 150 mM NaCl, 0.05% Tween-20 and 0.5 mM TCEP). Beads were extensively washed, eluted with binding buffer supplemented with 10 mM maltose and analyzed by SDS-PAGE gel electrophoresis.

Electron microscopy data collection

Purified separase-securin complexes were applied onto graphene oxide covered gold 300 square mesh Quantifoil R1.2/1.3 holey-carbon grids (Quantifoil Micro Tools GmbH) at a concentration of 100-200 nM. Graphene oxide grids were prepared as in Boland *et al.*[7] and https://figshare.com/articles/Graphene_Oxide_Grid_Preparation/3178669[37].

The grids were incubated for 10 s and back blotted for 3 s with 1 mm additional movement (90% humidity at 20 °C), before being plunged into liquid ethane using an EM GP2 automatic plunge freezer (Leica). Freshly purified securin$^{\Delta 160}$-separase^{C2029S}-Cdk1-cyclin B1-Cks1 complexes were dispensed onto graphene oxide covered Quantifoil R1.2/1.3 or R 2/2 holey-carbon grids at a concentration of 200-300 nM. Grids were similarly prepared using an EM GP2 automatic plunge freezer (Leica). The grids were stored in liquid nitrogen until further use.

Collection of dataset I of the separase-securin complex was described in ref.[7]. Dataset II was acquired on a Titan Krios electron microscope (Thermo Fisher Scientific). A total of 12,962 movies were recorded on a K3 camera (Gatan) operated in super-resolution mode, at a nominal magnification of 105,000, resulting in a super-resolution pixel size of 0.45 Å. A post-column energy filter was used for zero-loss filtration with an energy width of 20 eV. A total electron exposure of 67 $e^{-}/Å^2$ was distributed over 60 frames. Data were collected using the automated data collection software EPU (Thermo Fisher Scientific), with 4 acquisitions per hole and a set defocus range of −1.3 to −2.5 μm.

The cryoEM data of the securin$^{\Delta 160}$-separase^{C2029S}-Cdk1-cyclin B1-Cks1 complex were acquired on a Cs-corrected Titan Krios electron microscope (Thermo Fisher scientific) equipped with a Gatan K3 camera. A total of 13,640 super-resolution movies were recorded using EPU at a nominal magnification of 81,000, resulting in a super-resolution pixel size of

0.44 Å, and an energy filter slit width of 15 eV. A total electron exposure of 78 $e^{-}/Å^2$ was distributed over 60 frames per acquisition, at three acquisitions per hole and a set defocus range of −1.3 to −2.5 μm. Data acquisition was monitored by on-the-fly pre-processing using TranSPHIRE[38], including drift correction in MotionCorr2[39], CTF estimation in CTFFIND4[40], particle picking using a generalized neural network in SPHIRE-crYOLO[41] and 2D classification in ISAC[42].

Image processing

For the separase-securin complex, raw movies from both datasets were aligned and dose-weighed using MotionCorr2. Micrographs from dataset I have a pixel size of 1.05 Å, and micrographs of dataset II were two times binned, resulting in a pixel size of 0.90 Å. The two datasets were processed independently for Bayesian polishing and CTF refinement and combined according to Wilkinson *et al.*[43] for further processing. Micrographs were imported into CryoSPARC v2.14.2[44] and CTF parameters were estimated by Patch CTF estimation. Manually picked particles from a small subset of approximately 200 micrographs, followed by 2D classification, were used to train Topaz[45] or crYOLO for automated particle picking. The trained models were applied to the entire datasets. Particles were first cleaned up by two rounds of 2D classification (~200,000 particles for dataset I and ~260,000 particles for dataset II). After an initial round of 3D refinement, particles were exported to RELION 3.1 for Bayesian polishing and CTF refinement[46]. Polished particles from both datasets were subjected to another round of 2D classification and 3D classification. Carefully selected particles subsets were subjected to another round of CTF refinement, which resulted in a 3D reconstruction with a final resolution of 2.95 Å. To further improve the resolution of the separase protease domain and TPR-like domains, particle subtraction was performed with a soft mask around the two domains followed by focused 3D refinement, resulting in an improved map yielding 2.88 Å resolution. To improve the reconstruction of the HEAT-repeat domain, a soft mask was applied followed by particle subtraction and 3D classification without alignment. Particles from one class with good density of the HEAT-repeat domain were selected, reverted to original particles and used as input for 3D refinement, generating a final 3D reconstruction of 2.93 Å. Afterwards, the maps were postprocessed by deepEMhancer[47].

For the securin$^{\Delta 160}$-separase^{C2029S}-Cdk1-cyclin B1-Cks1 complex, the processing strategies were similar to those described above, resulting in a reconstruction with an overall resolution of 3.64 Å. All resolution estimations were derived from Fourier Shell Correlation (FSC) calculations between reconstructions from two independently refined half-sets, and reported resolutions are based on the FSC = 0.143 criterion. Local resolution was estimated with ResMap[48].

Model building and refinement

Ab initio model building of the human separase-securin complex was started using *Map to Model* in PHENIX[49]. The model was then manually built in Coot[50] iteratively and real-space refined using PHENIX. *C. elegans* separase-securin complex structure (PDB: 5MZ6[7]) served as a reference for modelling the separase protease domain and TPR-like domain. For modelling of the securin$^{\Delta 160}$-separase^{C2029S}-Cdk1-cyclin B1-Cks1 complex, the crystal

structure of Cdk1-cyclin B1-Cks2 (PDB: 4YC3[51]) and human separase structure were fitted into the density map and refined using Flex-EM[52] in CCPEM. Afterwards, the model was manually built in Coot iteratively and real-space refined using PHENIX. Model validation was performed with MolProbity[53,54]. Structural images were generated by Chimera[55] and Chimera X[56].

Data Availability

The EM maps are deposited with the Electron Microscopy Data Bank (EMDB) under accession code EMD-12368 and EMD-12369 for the separase-CCC and separase-securin complex, respectively. Protein coordinates of separase-CCC and separase-securin are deposited with the Protein Data Bank (PDB) under accession code 7NJ0 and 7NJ1, respectively.

Extended Data

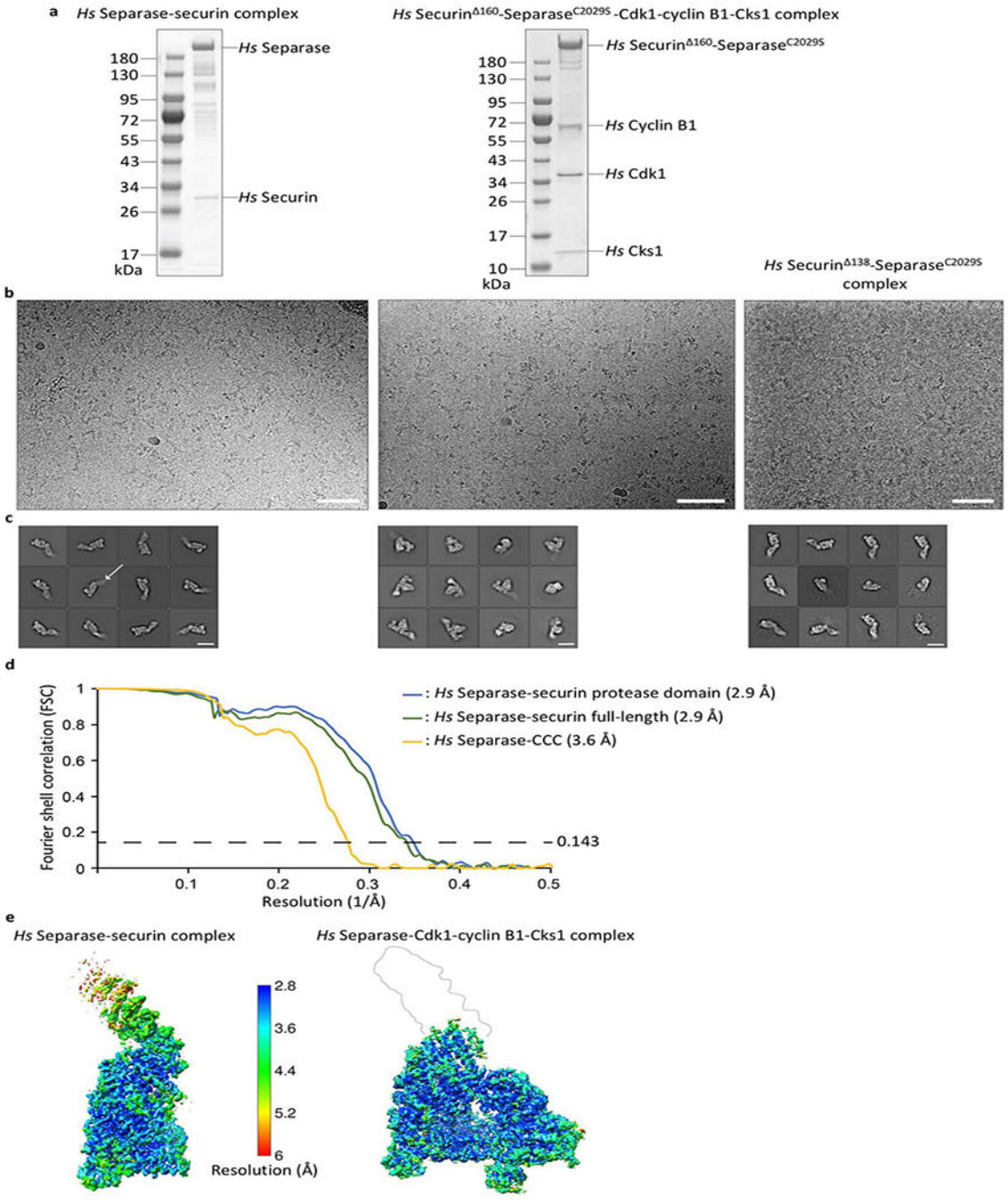

Extended Data Fig. 1. Preparations and EM images of the human separase-securin and separase-CCC complexes.

(a) SDS PAGE gels of wild-type *Hs* separase-securin and *Hs* securin$^{\Delta 160}$-separase^{C2029S}-Cdk1-cyclin B1-Cks1. **(b)** Representative cryo-electron micrographs of *Hs* separase-securin (left), *Hs* securin$^{\Delta 160}$-separase^{C2029S}-CCC (middle), and *Hs* securin$^{\Delta 138}$-separase^{C2029S} (right) collected on graphene oxide-coated EM grids. The scale bar corresponds to 500 Å. **(c)** Gallery of two-dimensional class averages of *Hs* separase-securin (left), *Hs* securin$^{\Delta 160}$-

separase^{C2029S}-CCC (middle) and *Hs* securin$^{\Delta 138}$-separase^{C2029S} (right) showing typical classes. The white arrow points at the flexible N-terminal HEAT-repeat domain. The white scale bar corresponds to 100 Å. To increase the number of views of separase in complex with either securin or the CCC complex, we used graphene oxide-coated electron microscopy (EM) grids as described[7,37]. We employed deep-learning software packages TOPAZ[45] and crYOLO[41] to establish reliable particle picking conditions that allowed the identification of rare particle projections. **(d)** Gold standard Fourier Shell Correlation (FSC) curve for full-length separase-securin, focused refined separase-securin C-terminal domains (TPR-like and protease domains) and securin$^{\Delta 160}$-separase^{C2029S}-CCC complexes. **(e)** EM density maps color-coded according to local resolution ranging from 2.8 Å to 6 Å.

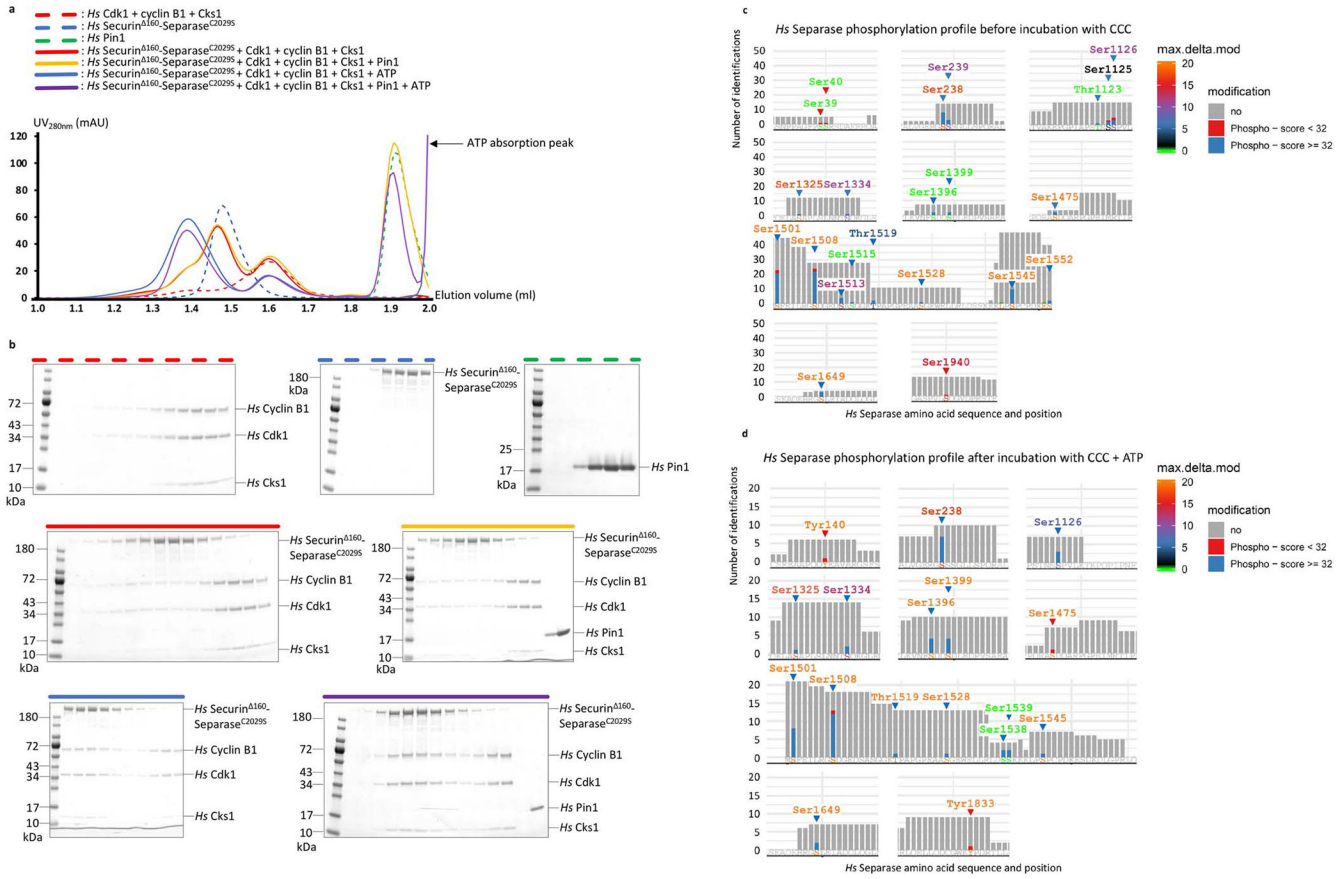

Extended Data Fig. 2. Evaluation of complex formation by size exclusion chromatography (SEC).

(a) Size exclusion chromatography (SEC) runs on the isolated Pin1, securin$^{\Delta 160}$-separase^{C2029S} and Cdk1-cyclin B1-Cks1 complexes resulted in elution volumes of approximately 1.9 ml, 1.5 ml and 1.6 ml, respectively (green, blue and red dashed lines). Adding the Cdk1-cyclin B1-Cks1 complex (CCC) to securin$^{\Delta 160}$-separase^{C2029S} did not yield a stable interaction between these two complexes under these conditions (red solid line). Adding Pin1 to the securin$^{\Delta 160}$-separase^{C2029S} complex in presence of CCC did not result in a detectable interaction of these two complexes (yellow solid line). However, a shoulder at high molecular weight can be observed indicating partial phosphorylation in insect cells, in accordance with our mass spectrometry results in **c**. Adding ATP to

securin$^{\Delta 160}$-separase^{C2029S}, Pin1 and CCC resulted in a clear shift to a 1.35 ml elution volume (purple solid line). A clear shift is also observed when adding ATP to securin$^{\Delta 160}$-separase^{C2029S} and CCC, indicating that Pin1 is dispensable for complex formation *in vitro* (blue solid line). **(b)** Coomassie Blue-stained polyacrylamide gels of fractions from the SEC runs. **(c)** Mass spectrometry analysis of human separase, without the CCC complex, shows phosphorylation of numerous sites in separase, including Ser1126. Each vertical bar indicates the number of times a peptide containing that site was identified, colored to indicate the presence of phosphorylation: for Ser1126, blue segments indicate high-confidence assignment of phosphorylation (Mascot peptide score >32) at three peptides, and red segments indicate lower scores at two peptides. The color of the amino acid label indicates the Mascot maximum delta mod score; a score of 10 for Ser1126 indicates high-confidence assignment of phosphorylation to that residue. **(d)** Mass spectrometry analysis of human separase after incubation with 5 mM ATP, 10 mM Mg^{2+} and the CCC complex also shows phosphorylation of separase Ser1126, with three high-confidence peptides (score>32) and maximum delta mod score of 8, also indicating a high-confidence assignment. Note that this analysis does not allow a rigorous quantitative comparison of Ser1126 phosphorylation in the two preparations.

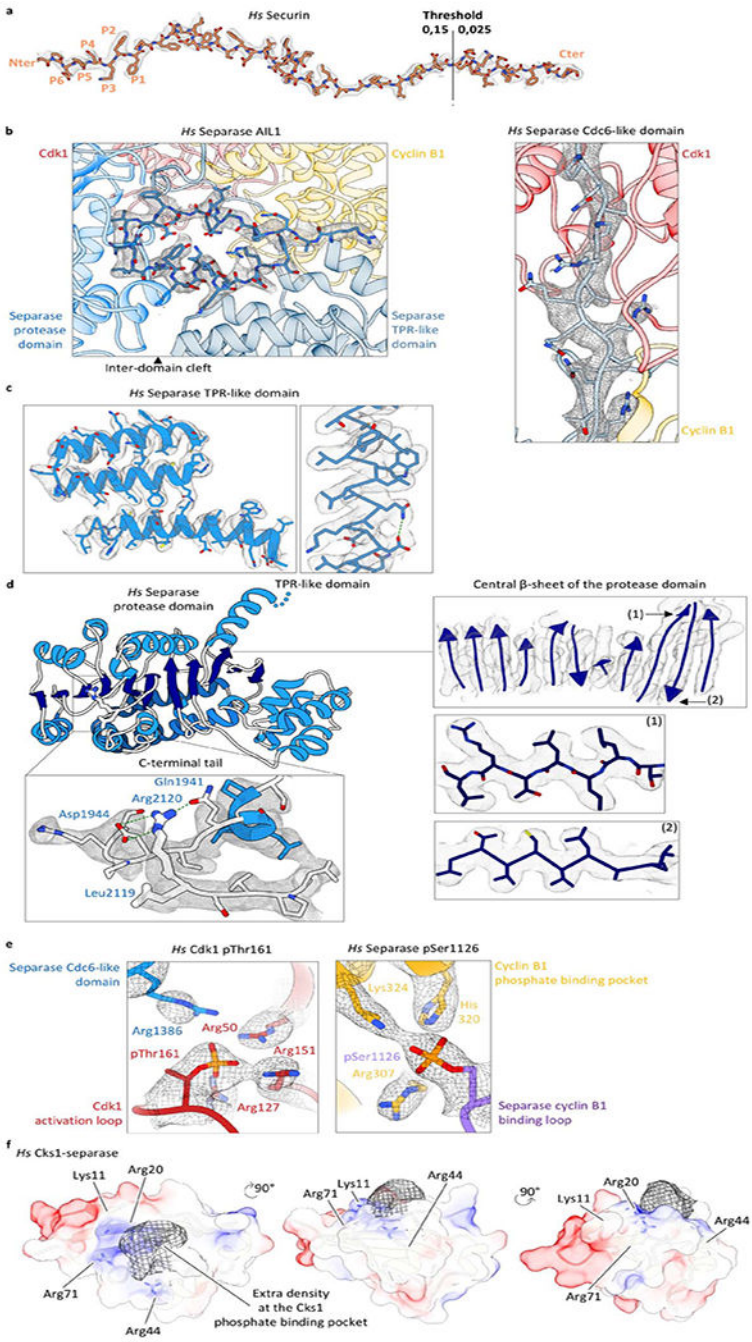

Extended Data Fig. 3. Representative EM density for *ab initio* model building.

(a) Securin density at different threshold levels (stronger information at the N-terminus of securin). Side-chain density is clearly visible. **(b)** Density of AIL1 located in a cleft between the TPR-like and protease domains (left) and the Cdc6-like domain of insert 2 (right). EM density allows the unambiguous placement of side chains in both loop segments. **(c)** Density of the TPR-like domain of human separase. **(d)** Examples of EM map quality for the separase protease domain. **(e)** Strong density of phosphothreonine 161 in Cdk1 (left) and

the separase phosphoserine 1126 of the cyclin B1-binding loop (right). **(e)** Extra density of human Cks1, possibly due to binding of phosphorylated threonine 1346 of separase.

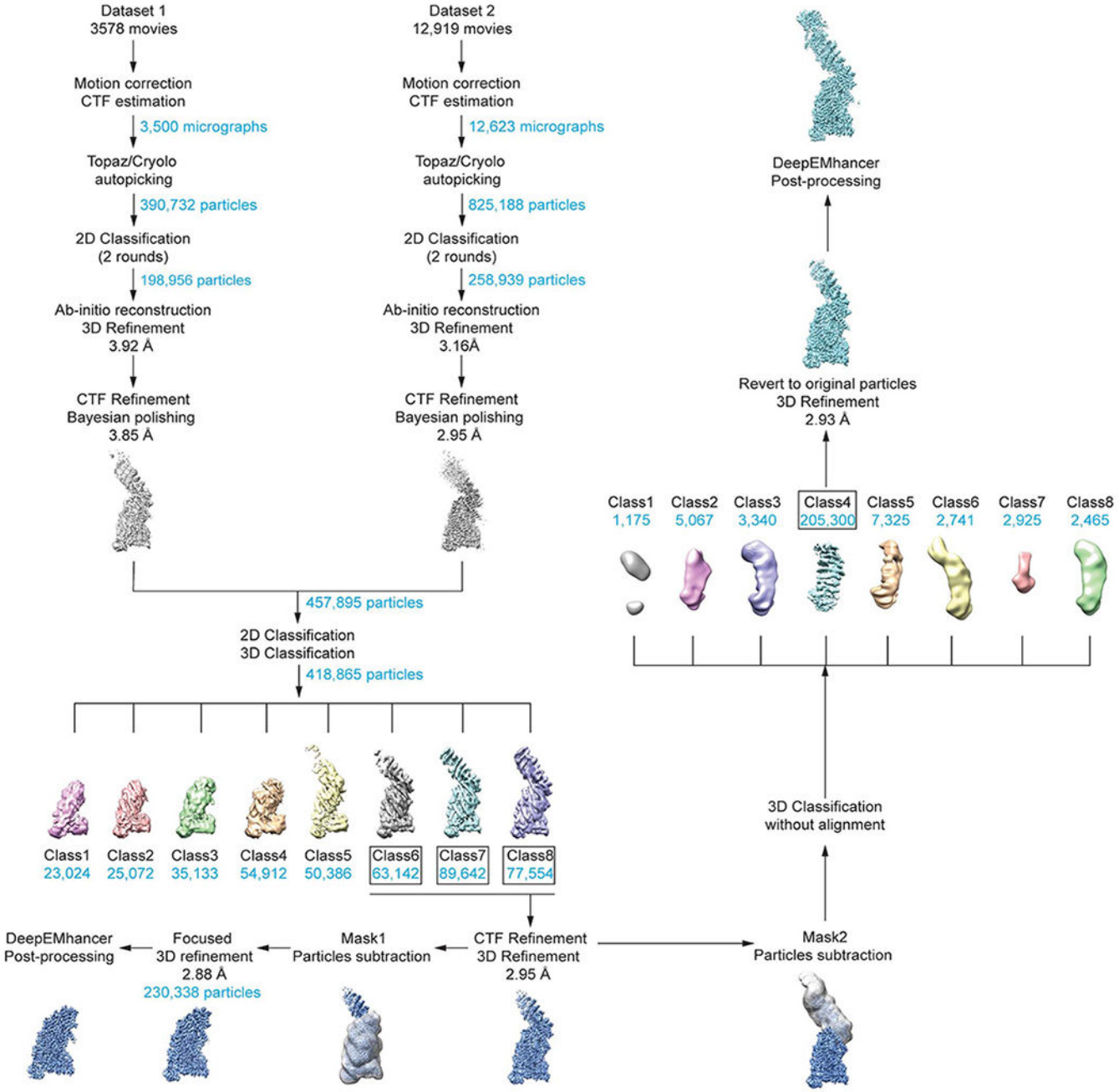

Extended Data Fig. 4. Data processing flowchart for the two datasets of the human separase-securin complex.

See Methods for details. 3D classification of separase-securin complexes resulted in about ~55% of particles with strong density for the N-terminal HEAT-repeat domain. These particles were subjected to CTF refinement and classified either on the N- or C-terminus. We used the particle subtraction for further classification. Classification on the N-terminal

domain was executed without alignment (in contrast to the larger C-terminal part) and resulted in approx. 200,000 particles that were used for a final 3D reconstruction. In both cases, DeepEMhancer[47] was used for post-processing.

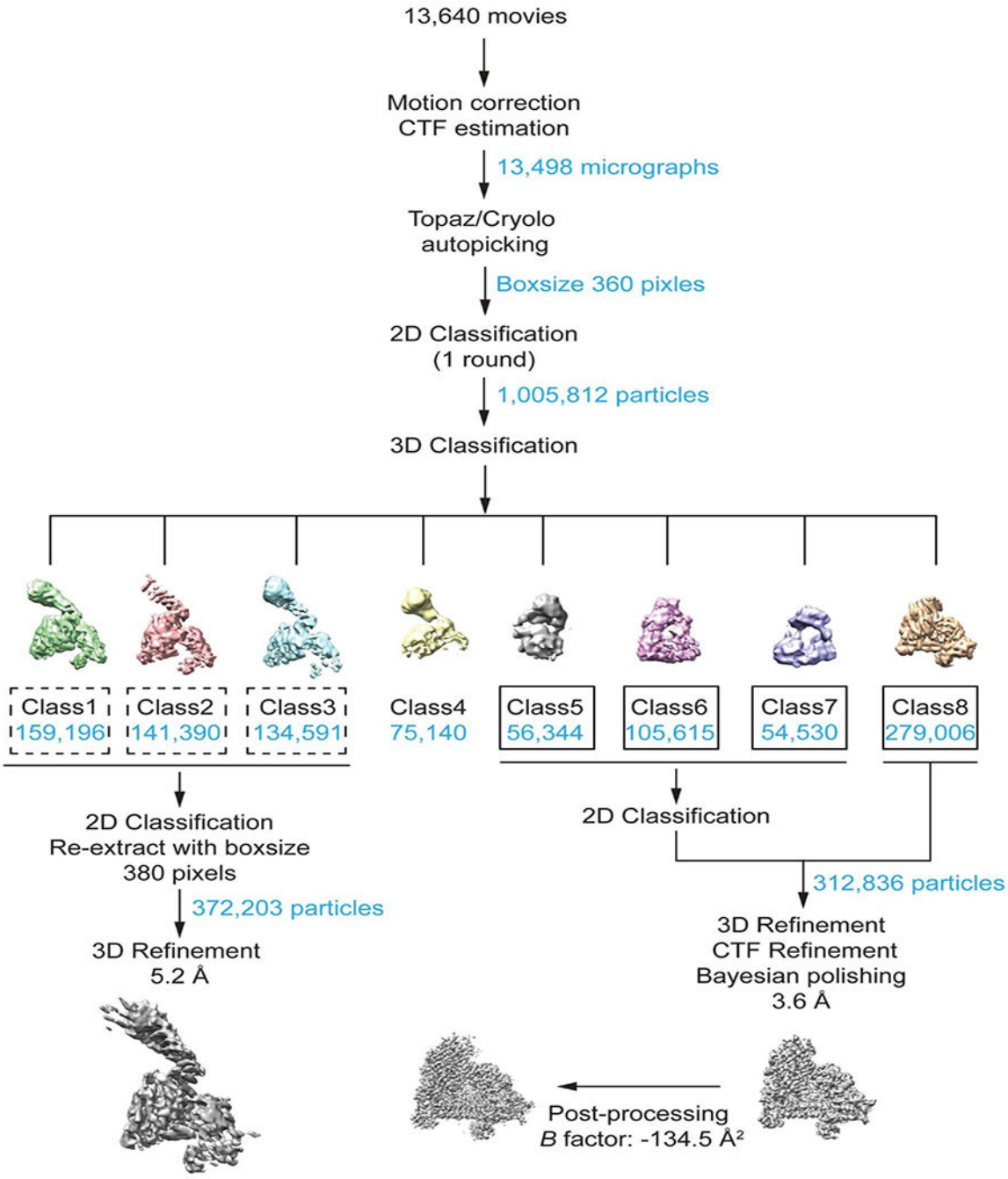

Extended Data Fig. 5. Data processing flowchart of the human separase-CCC complex.
See Methods for details. 3D classification of securin$^{\Delta 160}$-separase^{C2029S}-CCC complexes resulted in approximately 312,000 particles subjected to CTF refinement and Bayesian

polishing. The final reconstruction refined to roughly 3.6 Å resolution and was post-processed in RELION.

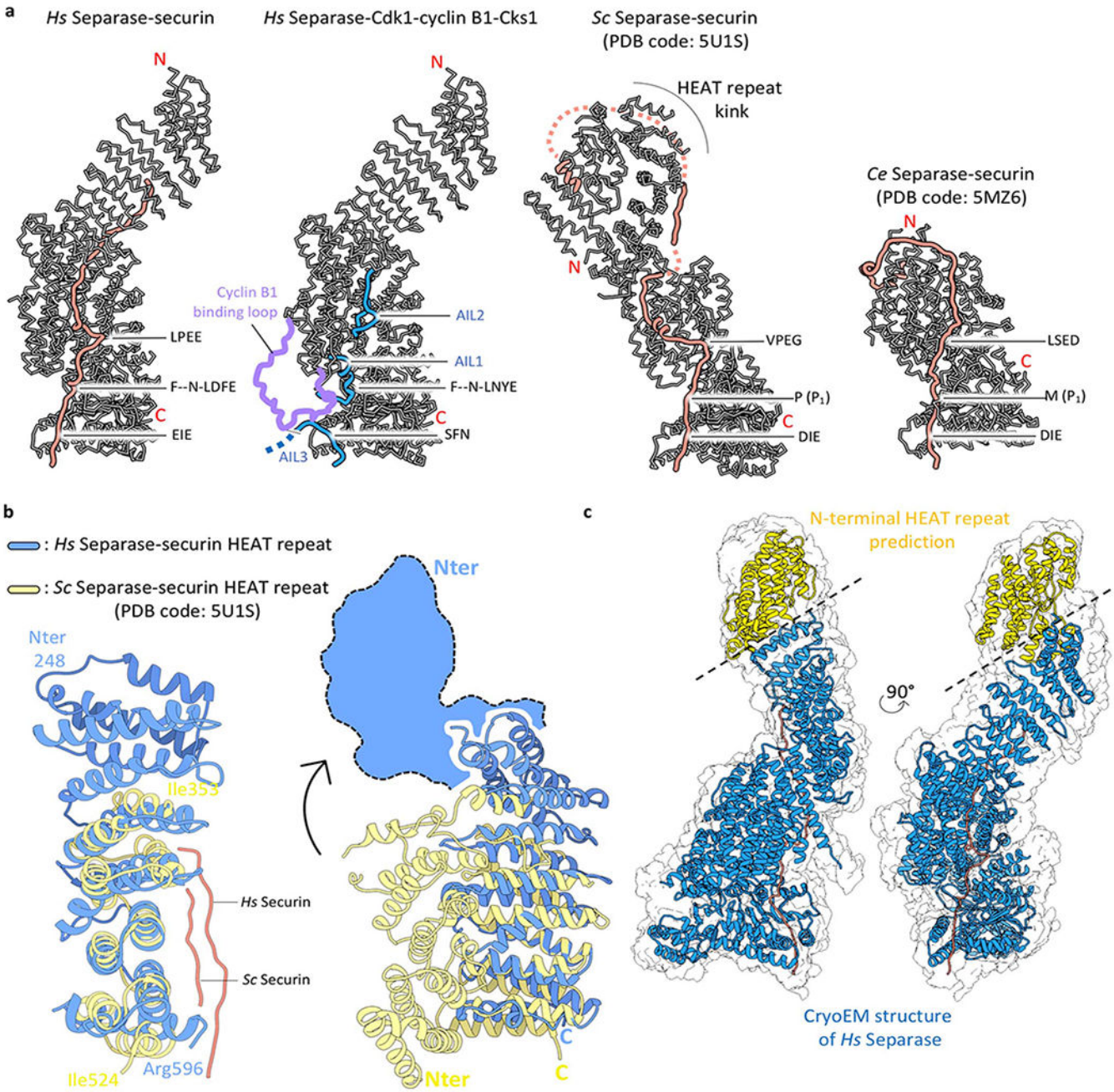

Extended Data Fig. 6. Comparison of flexible elements in separase proteins.

(a) Comparison of human separase in complex with securin or CCC to budding yeast (Sc) and *C. elegans* (*Ce*) separase. The loops AIL1, AIL2, AIL3 (highlighted in blue) as well as the cyclin B-binding loop (highlighted in purple) become ordered upon binding of CCC. The N-terminal domain adopts an elongated shape in human separase (two left structures) but in yeast this N-terminal domain is kinked. This domain is lost in *C. elegans* separase.

(b) Comparison of the N-terminal domains of human and yeast separases, with EM density for the first approx. 250 residues of human separase indicated as blue cartoon. The yeast N-terminal domain adopts a much more compact fold, with the N-terminus of the yeast protein folding back in close proximity to the TPR-like domain. This folded architecture may be an intrinsic feature of the yeast N-terminal domain or due to crystal packing constraints **(c)** EM density of human separase-securin at low threshold rendering allows a full representation of the enzyme (grey envelope). A predicted model of the N-terminal 250 residues is shown in yellow, and the EM-derived structure of separase-securin is shown in blue and orange, respectively.

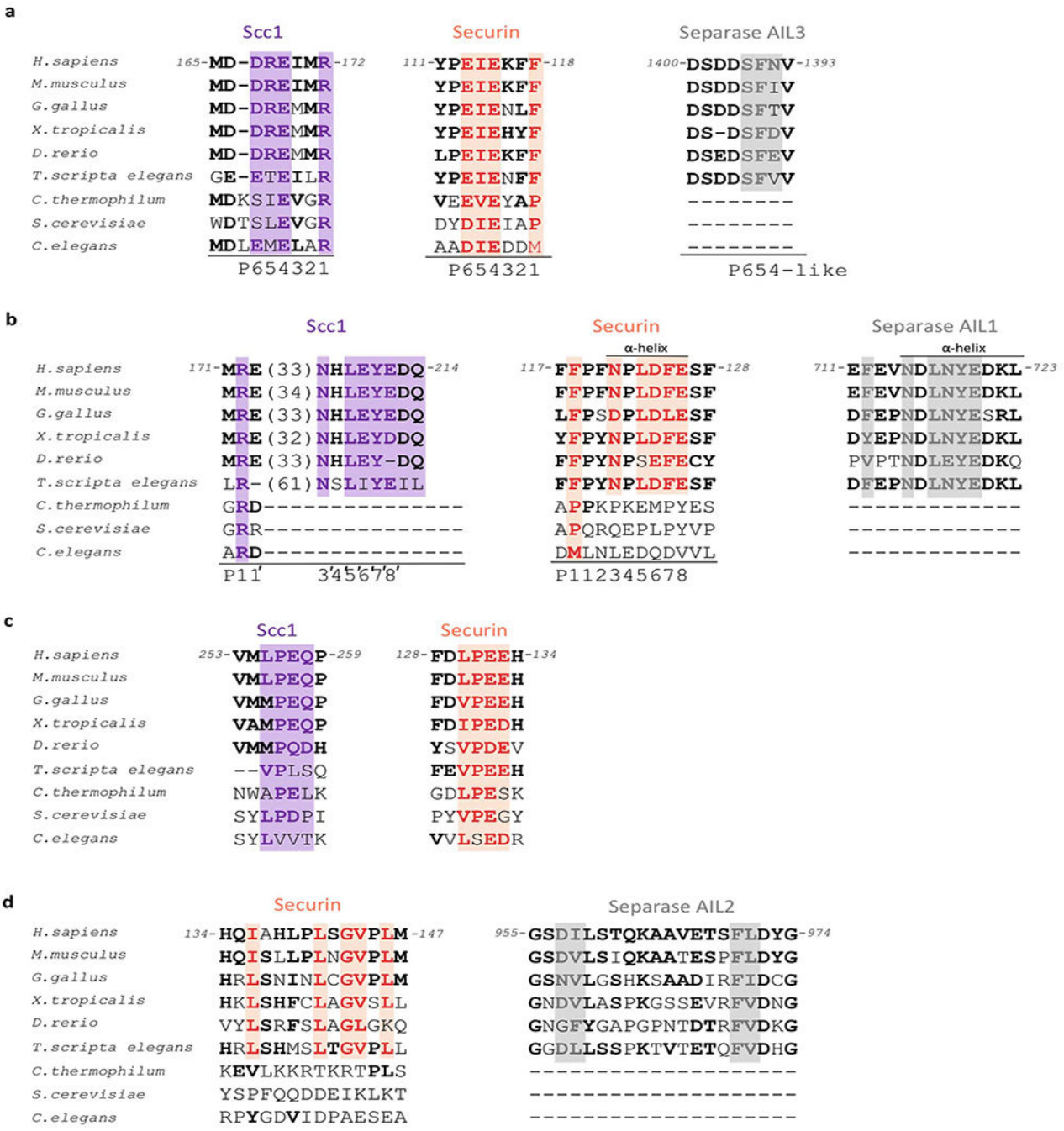

Extended Data Fig. 7. Multiple sequence alignments of conserved docking motifs in Scc1, securin and autoinhibitory loops of separase.

(a) Sequence comparison of the catalytic site binding motif in Scc1 (purple), securin (orange) and the AIL3 of separase (grey) in different species. Key residues are boxed. The invariant arginine residue involved in substrate catalysis (Scc1) is replaced by a large hydrophobic residue in securin. **(b)** Sequence comparison of the NxLxΦE binding motif in Scc1, securin and AIL1 of separase. A phenylalanine three amino acids upstream of the docking motif might correspond to the P1 position in Scc1 (arginine) or securin

(hydrophobic residue). **(c)** Sequence comparison of the LPE docking motif in Scc1 and securin. **(d)** Residues in securin and AIL2 of separase that bind to a hydrophobic cleft situated in the TPR-like domain of separase. See also Extended Data Fig. 11a.

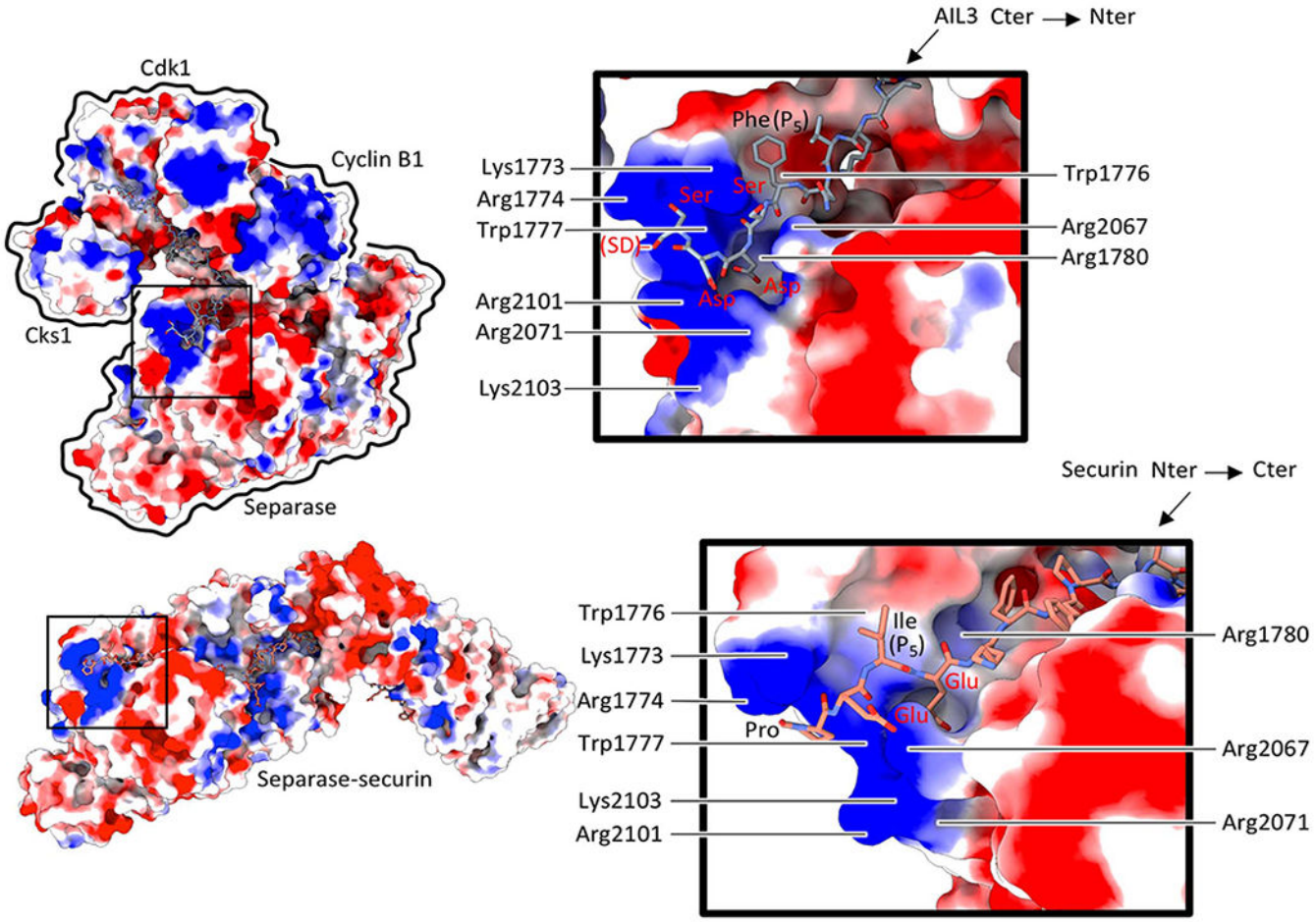

Separase sequence alignement

```
H.sapiens       1772-DKREWWTGRL(284)DRDIDRY(27)PRLKY-2104
M.musculus           EKRVWWTGRL(287)DRDIDRY(27)PRLKY
G.gallus             EKRAWWLCRF(283)DRDIDRY(28)PRLQH
T.scripta elegans    DKRDWWLGRT(284)DRDIDRY(27)PKLKY
X.tropicalis         DKKEWWEGRM(284)DREIDRY(27)PKLKY
D.rerio              EKSQWWDGRK(278)DRDLDRF(27)THLKH
C.thermophilum       EREKWWAERE(345)DRDIDRF(42)CRFRY
S.cerevisiae         ERKSWWTTRY(311)DKDIDKF(34)CHLRY
C.elegans            TPEEFWKRRK(288)DGEIDRF(34)ARLKY
```

Extended Data Fig. 8. Molecular surface charge representation of the separase-securin and separase-Cdk1-cyclin B1 complexes.

Surface charge of separase reveals a basic groove near the catalytic site that facilitates AIL3 (top) and securin (bottom) binding. Note that AIL3 binds in an inverted orientation to separase when compared to Scc1 or securin. Scc1 phosphorylation at a nearby serine

residue stimulates binding to this basic groove in yeast separase[23]. Phosphorylation of serine residues in AIL3 has been detected in other studies[19,30]. Sequence alignment (below) of the separase protease domain reveals conservation of residues critical for substrate or inhibitor recognition (boxed in grey).

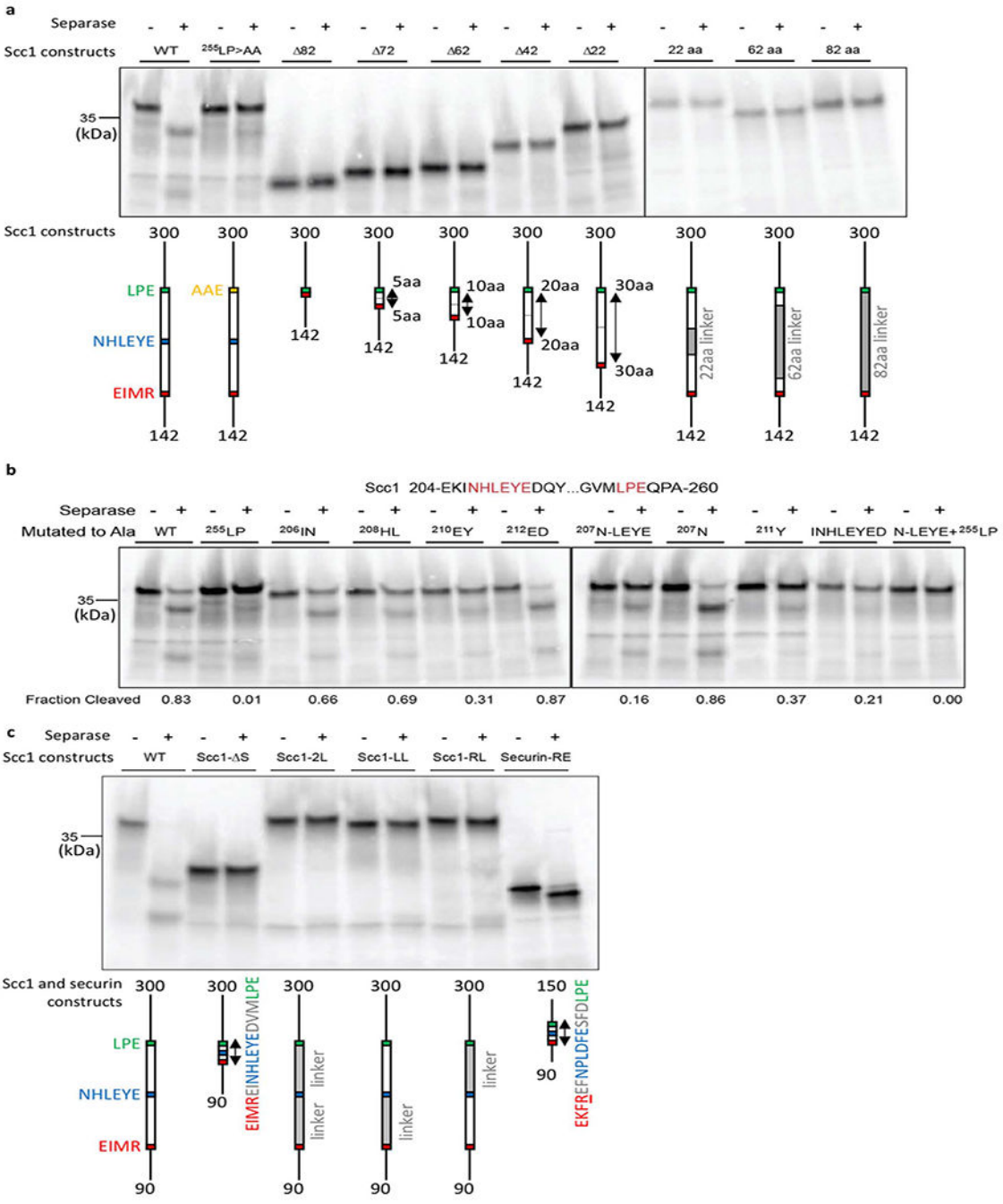

Extended Data Fig. 9. Scc1 cleavage is enhanced by the NHLEYE motif downstream of the cleavage site.

(a) Scc1 deletion mutants (left gel) were constructed to test the function of the 82 amino acid region between the cleavage site ([169]EIMR) and the [255]LPE docking site. Constructs

were made in an internal Scc1 fragment (residues 142-300). Each construct removed from 22 to 82 residues around the center of the intervening region, as indicated in the diagrams. In another series of constructs (right gel), different amounts of the intervening sequence were replaced with random linker sequence (G, S, A, and T). ^{35}S-labeled Scc1 fragments were incubated with or without separase, and reaction products were analyzed by SDS-PAGE and Phosphorimaging. The central 22-amino acid region contains the conserved ^{207}NHLEYE sequence. Results are representative of four independent experiments. **(b)** The indicated amino acids were replaced with alanine in Scc1 (residues 142-300). ^{35}S-labeled Scc1 mutants were incubated with or without separase, and reaction products were analyzed by SDS-PAGE and Phosphorimaging. Results are representative of four independent experiments. **(c)** In Scc1, 30-40 residue spacers separate the cleavage site (^{169}EIMR) and two docking sites (^{207}NHLEYE and ^{255}LPE). The importance of the spacer regions was tested with various mutations in an internal Scc1 fragment (residues 90-300). In the Scc1-ΔS mutant, both spacers were deleted. In the three linker mutants, the two intervening spacers were replaced, together or one at a time, with random linker sequence (G, S, A, and T). Results are representative of four independent experiments. The reaction at far right demonstrates cleavage of the securin-RE mutant (residues 93-150), in which the pseudosubstrate motif ^{115}EKF**FP** is converted to EKF**RE (ref.** ^{13}). Thus, closely-spaced docking motifs allow cleavage of securin but not that of Scc1.

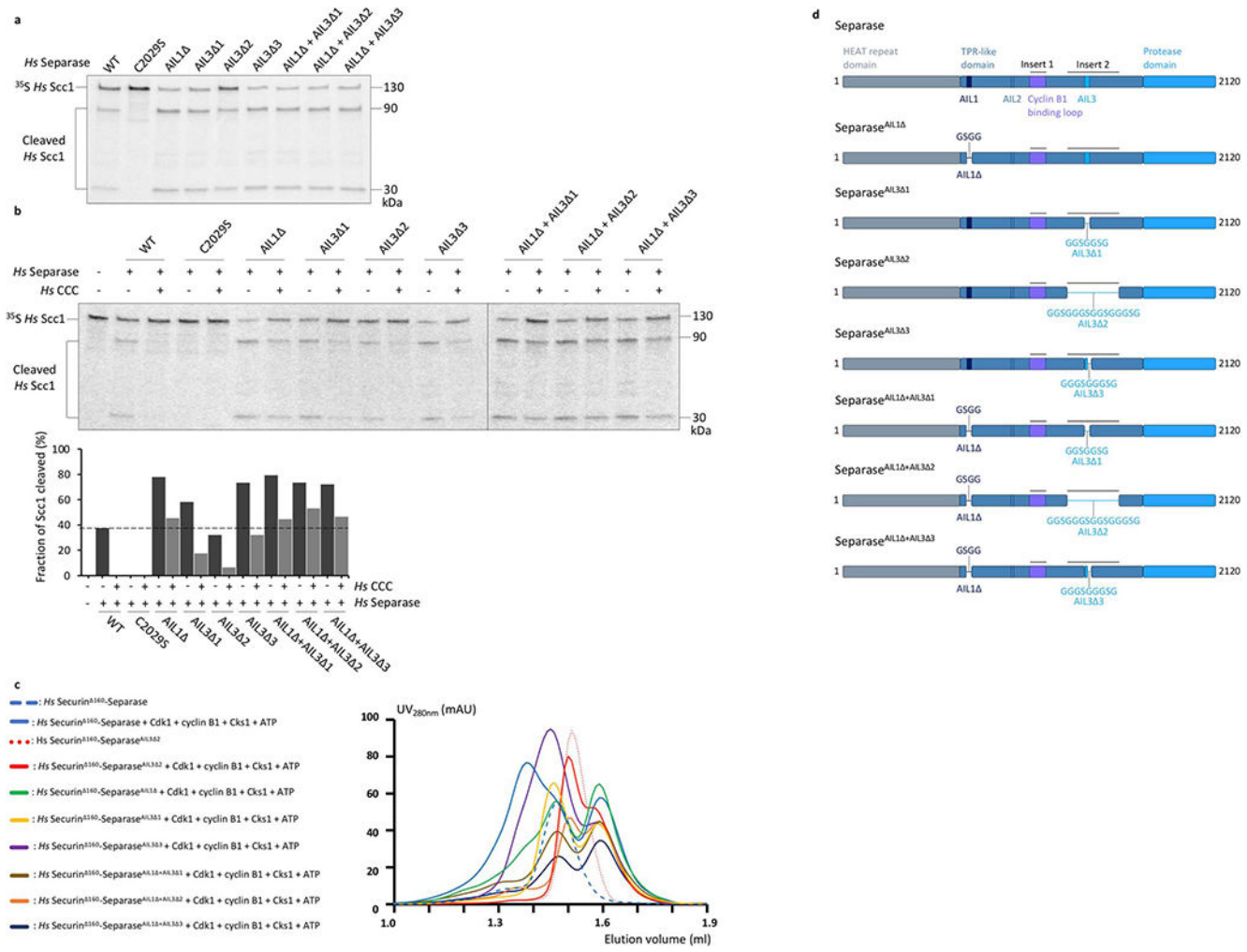

Extended Data Fig. 10. Loop deletions of AIL1 and AIL3 enhance separase cleavage activity.

(a) Separase mutants carrying deletions of AIL1 and/or AIL3 were purified to analyze the effect of these loop segments on separase cleavage activity. Results are representative of three independent experiments. Regions deleted in each mutant as follows (see Extended Data Table 2 for sequence details): AIL1Δ, deletion of AIL1, which harbors the NDLNYE motif; AIL3Δ1, deletion of Cdc6-like domain and NFS motif; AIL3Δ2, deletion of entire insert 2; AIL3Δ3, deletion of NFS motif. ^{35}S-labeled full-length Scc1 was incubated with either wild-type (WT) separase, an inactive separase mutant (C2029S), or separase loop deletions as indicated. Reaction products were analyzed by SDS-PAGE and Phosphorimaging. All loop deletions show enhanced Scc1 cleavage activity, with the exception of a mutant carrying a deletion of the entire insert 2, which exhibits cleavage activity comparable to that of the wild-type protein. Quantification of three independent experiments shown in Fig. 2g. **(b)** Full-length Scc1 cleavage assays as described in **(a)** in presence or absence of the CCC complex. Results are representative of three independent experiments. While Scc1 cleavage by wild-type separase is fully repressed by the CCC complex (lane 3), mutant proteins with deletions of AIL1 and/or AIL3 show partial cleavage activity in presence of the CCC complex. Deletion of insert 2 (AIL3Δ2) leads to lower

cleavage activity compared to other loop deletions. The reduction in inhibition by the CCC complex can be partially explained through reduced complex affinity as demonstrated by SEC runs shown in **(c)**. Only wild-type separase (solid blue line) shows a clear shift towards a higher molecular weight elution volume after incubation with 5 mM ATP, 10 mM Mg^{2+} and the CCC complex. **(d)** Schematic diagram of the loop mutants analyzed in these experiments.

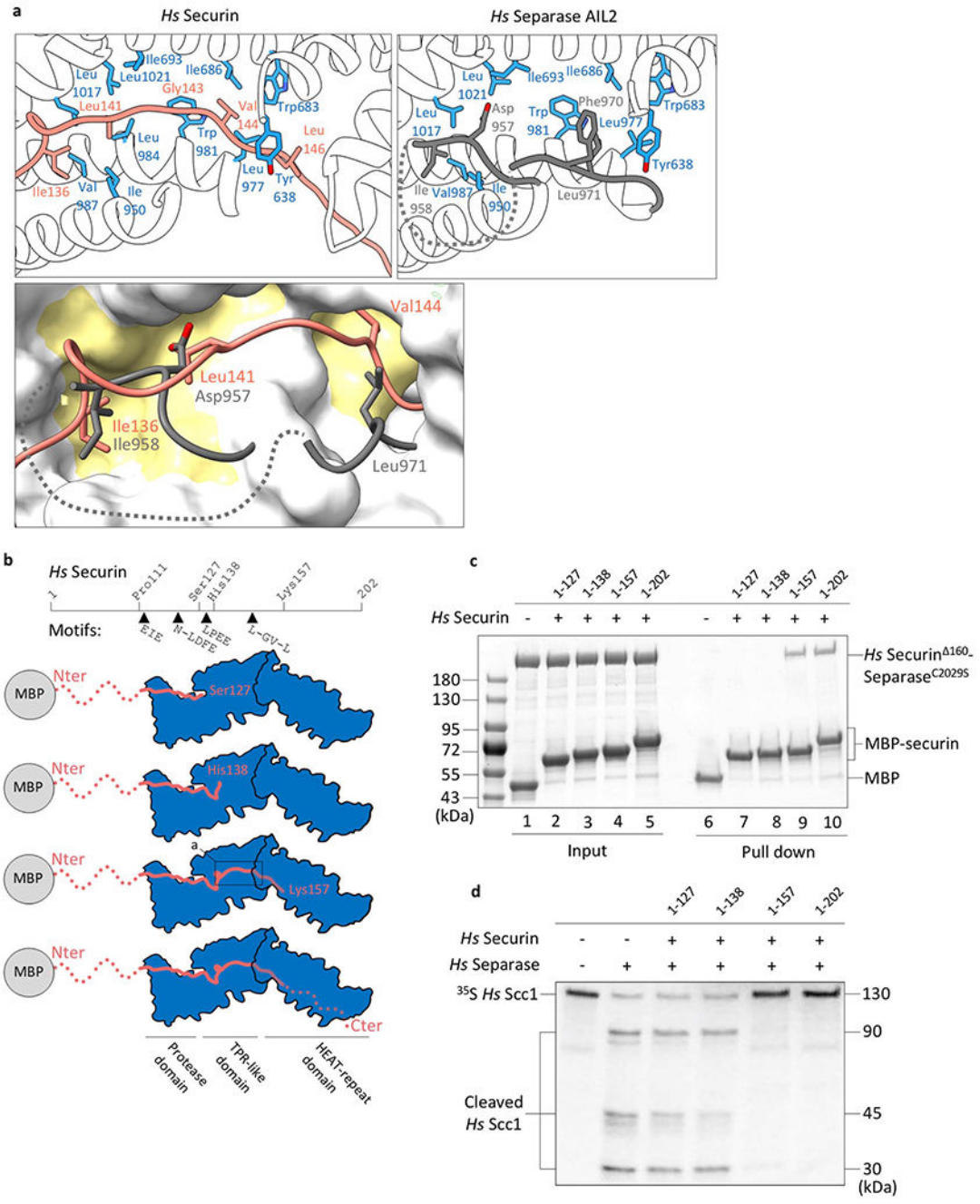

Extended Data Fig. 11. A hydrophobic cleft in separase promotes securin binding and correlates directly with substrate cleavage efficiency.

(a) Close-up of the binding interface of the hydrophobic cleft of separase interacting with securin (top left, orange) or the AIL2 of separase (top right, grey). The molecular surface representation (below) highlights the hydrophobic nature of the binding cleft in separase. **(b)** Schematic representation of constructs used in binding and cleavage assays. **(c)** *In vitro* pull-down assays using maltose binding protein (MBP)-securin fusions as bait demonstrates the importance of a stretch of hydrophobic amino acids in securin. A construct including residues 1-157 or wild-type securin (1-202) can bind to separase (lane 9 and 10), whereas two C-terminal truncations (securin$^{\Delta 127}$ and securin$^{\Delta 138}$) do not bind separase under these conditions (lane 7 and 8). Purified MBP serves as negative control (lane 6). Lane 1-5 are 10% of the input. Pull-down experiments have been repeated in three independent experiments. **(d)** ^{35}S-labeled full-length Scc1 proteins were incubated with or without separase, and reaction products were analyzed by SDS-PAGE and Phosphorimaging. Scc1 cleavage by separase is inhibited by addition of full-length securin 1-202 or truncated securin 1-157 (lane 5 and 6). Shorter securin constructs, securin 1-127 and securin 1-138, which lack a stretch of hydrophobic residues, do not inhibit cleavage under these conditions (lane 3 and 4).

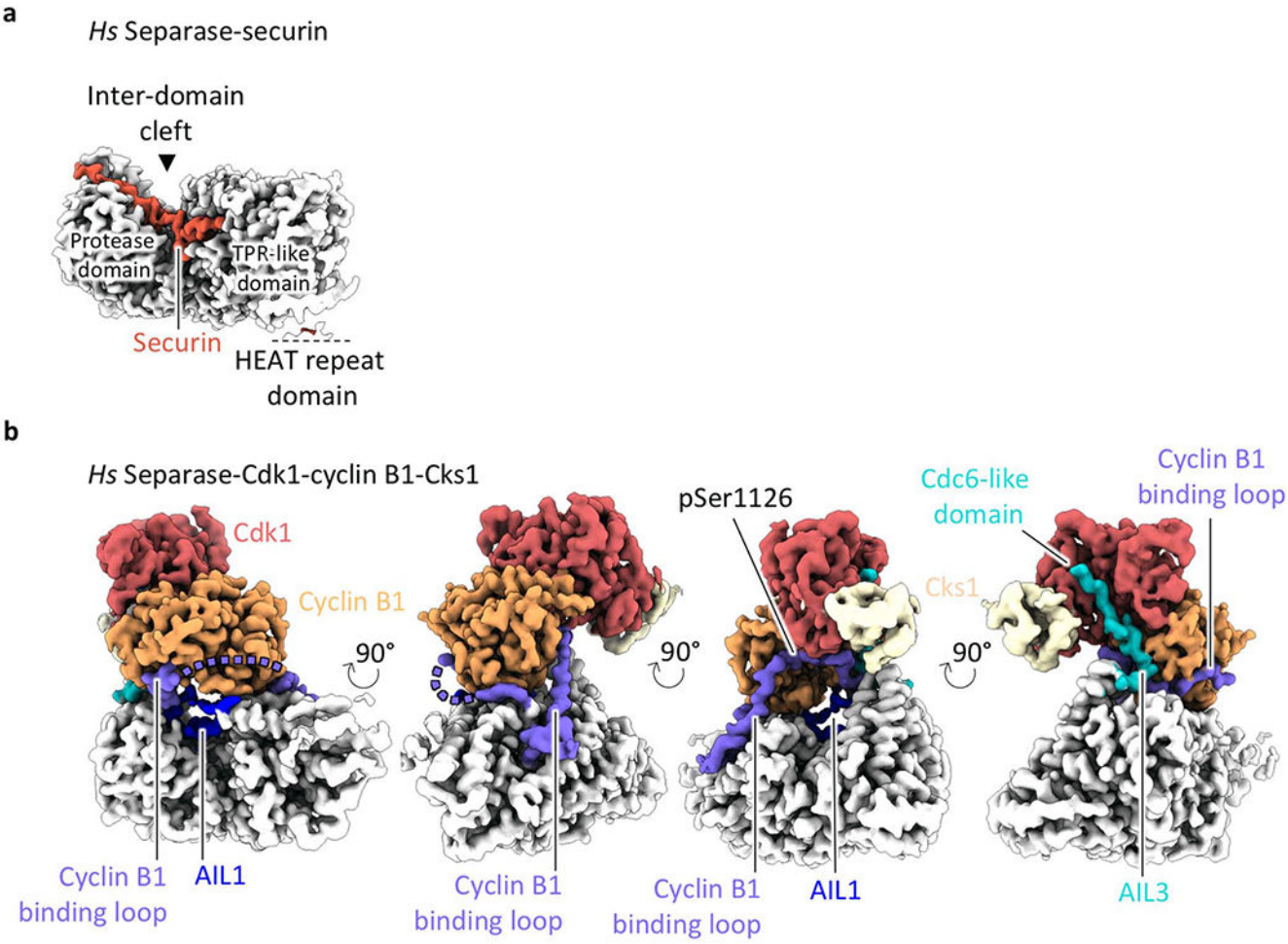

Extended Data Fig. 12. The Cdk1-cyclin B1-Cks1 complex binds to a clearly defined cleft in separase.

(a) The separase-securin complex has a clearly defined cleft between the TPR-like and protease domains. **(b)** The separase-CCC complex in four orientations (each rotated by 90°). The HEAT-repeat domain is omitted for clarity.

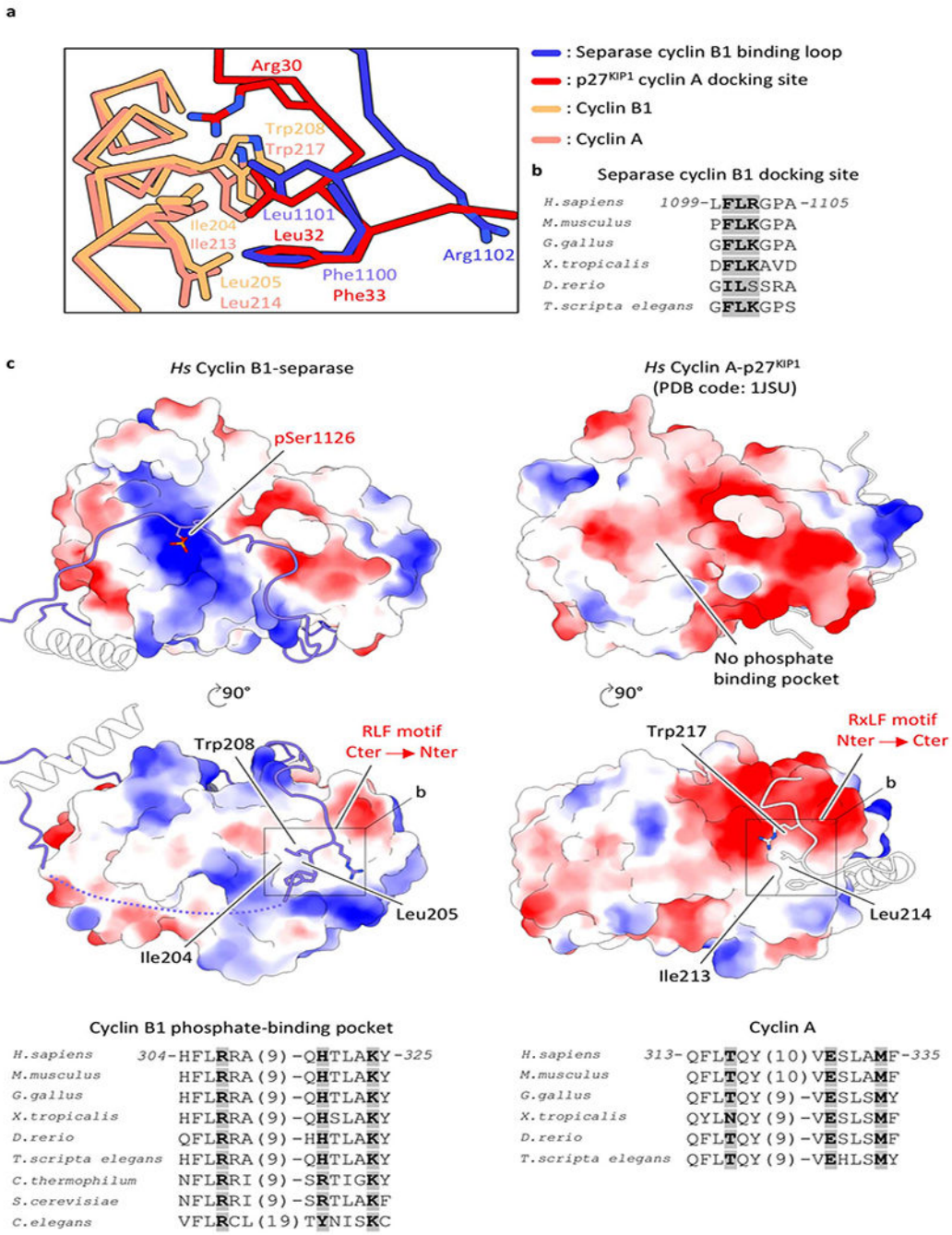

Extended Data Fig. 13. Molecular surface charge representation of cyclins.

(a) The cyclin B-binding loop of separase binds inverted to the substrate-docking hydrophobic patch of cyclin B1 when compared to common substrates. (**b**) Sequence

alignment of the cyclin B-binding loop docking site motif. **(c)** Calculating the surface charge of A- and B-type cyclins illustrates the existence of a phosphate-binding pocket in cyclin B1 but not cyclin A (compare top left versus top right). The cyclin B-binding loop also binds to the substrate-docking hydrophobic patch of cyclins B1 comparable to a typical cyclin B1-binding partner. Multiple sequence alignment of residues lining the phosphate-binding pocket shows conservation of Arg307, His320 and Lys324 in B-type cyclins (bottom left) but not in cyclin A (bottom right).

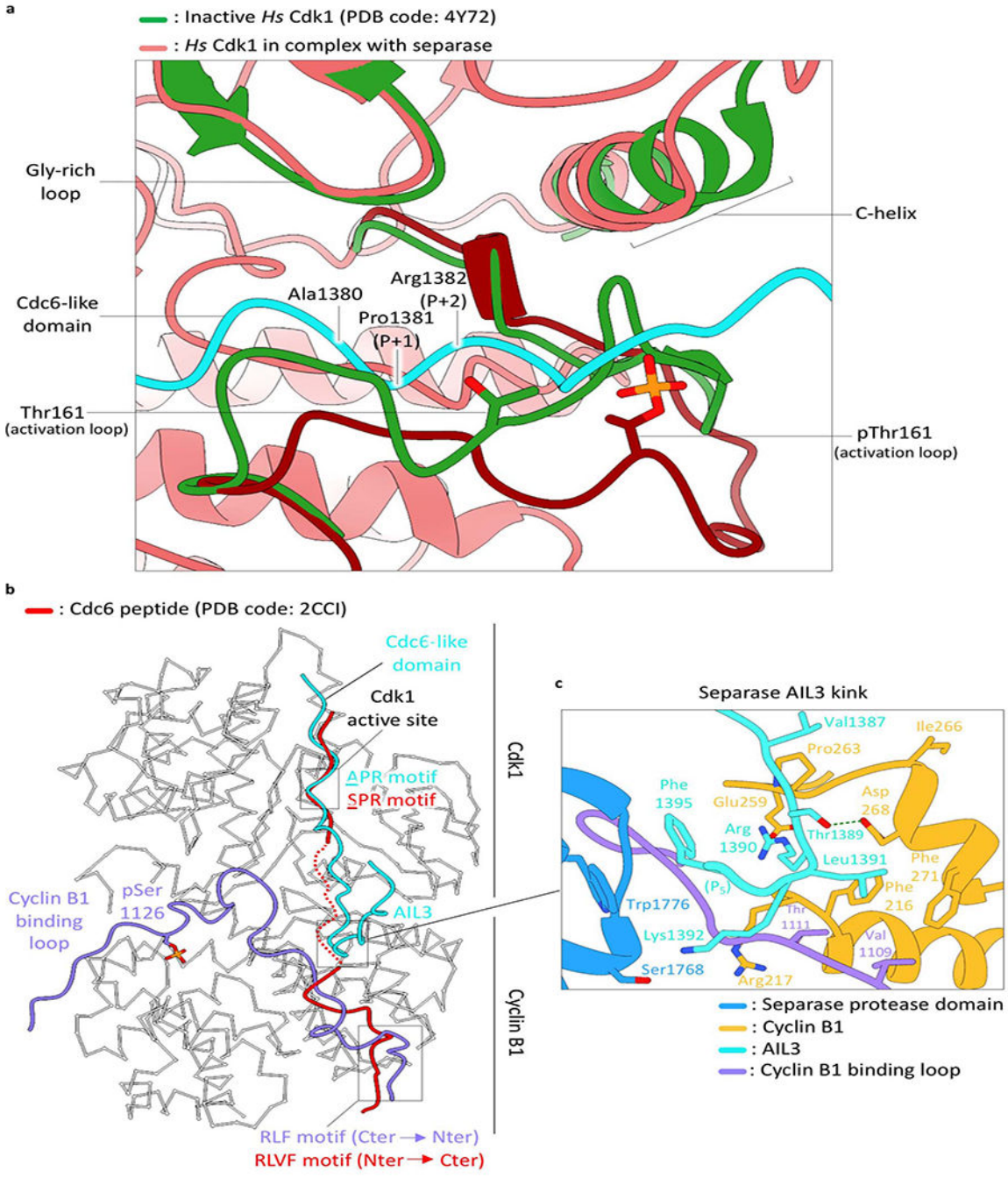

Extended Data Fig. 14. Binding of separase to Cdk1-cyclin B is mediated through two distinct loops.

(a) Comparison of human Cdk1 in a chemical inhibitor-bound state (green) and the separase-CCC complex (pale red) with the Cdc6-like domain of separase (AIL3; cyan). In the separase-CCC complex the activation loop is in its active conformation (downwards) and allows substrate and separase binding. In the inhibitor-bound structure the activation loop conformation is incompatible with substrate binding. **(b)** The Cdc6-like domain of separase binds to the active site of Cdk1, while the cyclin B-binding loop (purple) of separase wraps around cyclin B1 with pSer1126 in its center and hydrophobic patch interactions nearby. In common cyclin B substrates these interactions are mediated through one continuous polypeptide (red). **(c)** A kink in AIL3 is formed at the interface of cyclin B1 and the separase protease domain, with Thr1389, Arg1390 and Leu1391 being key residues for AIL3 binding to cyclin B1.

Extended Data Table 1

CryoEM data collection, refinement and validation statistics

	***Hs* Separase-securin Dataset 1**	***Hs* Separase-securin Dataset 2**	***Hs* Securin$^{\Delta 160}$-Separase^{C2029S}-Cdk1-cyclin B1-Cks1**	***Hs* Securin$^{\Delta 138}$-Separase^{C2029S}**
Data collection				
Microscope	FEI Titan Krios	FEI Titan Krios	FEI Titan Krios	FEI Titan Krios
Magnification	47,619	105,000	81,000	96,000
Voltage (keV)	300	300	300	300
Electron dose (e^{-}/Å^{-2})	40	67	78	59.7
Detector	Gatan K2 Summit	Gatan K3 Summit	Gatan K3 Summit	Falcon 4
Pixel size (Å/pixel)	1.05	0.90	0.88	0.681
Defocus range (μm)	1.0-3.0	1.3-2.5	1.3-2.5	1.0-2.5
Number of micrographs	3,578	12,962	13,640	2,901
Reconstruction				
Particles	205,300		312,836	
Box size (pix)	318		360	
Accuracy of rotations (°)	2.336		1.871	
Accuracy of translations (pix)	0.778		0.781	
Map sharpening B-factor (Å^2)	−78		−120	
Resolution (global, Å)	2.9		3.6	
Resolution range(local, Å)	2.9-6.0		3.6-4.8	
FSC threshold	0.143		0.143	
Model composition				
Protein residues	1,501		1,818	
Ligands	--		1	
Refinement				
Resolution (Å)	3.0		3.6	
FSC threshold	0.5		0.5	
Model to map scores -CC	0.76		0.84	

	Hs Separase-securin Dataset 1	*Hs* Separase-securin Dataset 2	*Hs* Securin$^{\Delta 160}$-Separase^{C2029S}-Cdk1-cyclin B1-Cks1	*Hs* Securin$^{\Delta 138}$-Separase^{C2029S}
B factors (Å^2)				
Protein residues	64.76		64.74	
Ligands	--		41.08	
R.m.s deviations				
Bond lengths (Å)	0.004		0.004	
Bong angles (°)	0.568		0.631	
Validation				
Clashscore, all atoms	9.30		6.72	
Rotamer outliers (%)	1.91		0.10	
Ramachandran plot				
Favoured (%)	92.20		91.13	
Allowed (%)	7.80		8.87	
Outliers (%)	0.00		0.00	
Deposition				
PDB ID	7NJ1		7NJ0	
EMDB ID	EMD-12369		EMD-12368	

Extended Data Table 2

List of proteins used in this study

Protein name	Tag	WT/Mutation/deletion			Experiments
		Description	Original sequence	Modified sequence	
Securin-Separase	C-terminal 2xStrep-tag (securin)	Wild-type complex	--	--	CryoEM data collection
Securin$^{1-127}$	N-terminal MBP-tag (securin)	C-terminal truncation	^{1}MATLI…CDIDI^{202}	^{1}MATLI…LDFES^{127}	Pull down and activity assays
Securin$^{1-138}$	N-terminal MBP-tag (securin)	C terminal truncation	^{1}MATLI…CDIDI^{202}	^{1}MATLI…HQIAH^{138}	Pull down and activity assays
Securin$^{1-157}$	N-terminal MBP-tag (securin)	C terminal truncation	^{1}MATLI…CDIDI^{202}	^{1}MATLI…RELEK^{157}	Pull down and activity assays
Securin$^{1-202}$	N-terminal MBP-tag (securin)	Wild-type	--	--	Pull down and activity assays
Securin$^{\Delta 160}$-Separase^{C2029S}	C-terminal 2xStrep-tag (separase)	Securin$^{160-202}$ fused to the N-terminus of separase; Catalytic	Cys2029	Ser2029	Assembly of separase-CCC complex; pull down assays

Protein name	Tag	WT/Mutation/deletion			Experiments
		Description	Original sequence	Modified sequence	
		inactive mutant			
Securin$^{\Delta 160}$-Separase	C-terminal 2xStrep-tag (separase)	Securin$^{160\text{-}202}$ fused to N terminus of separase	--	--	Activity assays
Securin$^{\Delta 138}$-Separase	--	Securin$^{138\text{-}202}$ fused to N-terminus of separase	--	--	Activity assays
Securin$^{\Delta 138}$-Separase^{C2029S}	--	Securin$^{138\text{-}202}$ fused to N-terminus of separase; Catalytically inactive mutant	--	--	CryoEM data collection
Cdk1-cyclin B1-Cks1 (CCC)	C-terminal 2xStrep-tag (cyclin B1); C-terminal 8xHis-tag (Cdk1)	Wild-type complex	--	--	Assembly of separase-CCC complex; activity assays
Securin$^{\Delta 160}$-Separase^{C2029S}-CCC	C-terminal 2xStrep-tag (separase); C-terminal 2xStrep-tag (cyclin B1); C-terminal 8xHis tag (Cdk1)	Securin$^{160\text{-}202}$ fused to N terminus of separase; Catalytically inactive mutant	Cys2029	Ser2029	CryoEM data collection
Pin1	--	Wild-type	--	--	Assembly of separase-CCC complex
Securin$^{\Delta 160}$-Separase$^{AIL1\Delta}$	2xStrep-tag (separase)	Securin$^{160\text{-}202}$ fused to N-terminus of separase; AlL1 loop deletion	^{705}APGNLE EFEVNDLNYE DKLQEDR^{727}	GSGG	Activity assays
Securin$^{\Delta 160}$-Separase$^{AIL3\Delta 1}$	2xStrep-tag (separase)	Securin$^{160\text{-}202}$ fused to N-terminus of separase; AlL3 loop deletion 1	^{1374}KPEVPQAPRVQQR VQTR LKVNFSDDSD^{1400}	GGSGGSG	Activity assays
Securin$^{\Delta 160}$-Separase $^{AIL3\Delta 2}$	2xStrep-tag (separase)	Securin$^{160\text{-}202}$ fused to N-terminus of separase; AlL3 loop deletion 2 (insertion 2)	^{1302}VPGSE… VATGL^{1571}	GGSGGGSGGSGG GSG	Activity assays

Protein name	Tag	WT/Mutation/deletion			Experiments
		Description	Original sequence	Modified sequence	
Securin$^{\Delta 160}$-Separase$^{AIL3\Delta 3}$	2xStrep-tag (separase)	Securin$^{160\text{-}202}$ fused to N-terminus of separase; AlL3 loop deletion 3	^{1392}KVNFSDDSD^{1400}	GGGSGGGSG	Activity assays
Securin$^{\Delta 160}$-Separase$^{AIL1\Delta+AIL3\Delta 1}$	2xStrep-tag (separase)	Securin$^{160\text{-}202}$ fused to N-terminus of separase; AlL1 loop deletion; AlL3 loop deletion 1	^{705}APGNLE EFEVNDLNYE DKLQEDR^{727}	GSGG	Activity assays
			^{1374}KPEVPQAPRVQQR VQTR LKVNFSDDSD^{1400}	GGSGGSG	
Securin$^{\Delta 160}$-Separase$^{AIL1\Delta+AIL3\Delta 2}$	2xStrep-tag (separase)	Securin$^{160\text{-}202}$ fused to N-terminus of separase; AlL1 loop deletion; AlL3 loop deletion 2 (insertion 2)	^{705}APGNLE EFEVNDLNYE DKLQEDR^{727}	GSGG	Activity assays
			^{1302}VPGSE… VATGL^{1571}	GGSGGGSGGSGG GSG	
Securin$^{\Delta 160}$-Separase$^{AIL1\Delta+AIL3\Delta 3}$	2xStrep-tag (separase)	Securin$^{160\text{-}202}$ fused to N-terminus of separase; AlL1 loop deletion; AlL3 loop deletion 3	^{705}APGNLE EFEVNDLNYE DKLQEDR^{727}	GSGG	Activity assays
			^{1392}KVNFSDDSD^{1400}	GGGSGGGSG	
Plk1$^{37\text{-}345}$	--	Human Plk1 fragment	--	--	Activity assays

Supplementary Material

Refer to Web version on PubMed Central for supplementary material.

Acknowledgements

We thank Yvan Pfister and Isabelle Flückinger for excellent technical assistance and Anna Katharina Höfler and Lina Poulain for critical input and helpful discussions. We thank Julia Kamenz, Robbie Loewith and Florian Steiner for critical reading of the manuscript. We thank Jing Yang and Ziguo Zhang for assistance in the early stages of this project; Oliver Hofnagel and Daniel Prumbaum for excellent assistance with EM data collection at the Max Planck Institute of Molecular Physiology; Claudio Alfieri for sharing his PLK1 plasmid; the computing department of the University of Geneva for providing an excellent infrastructure to perform cryoEM analysis and Nicolas Roggli for maintaining computing in the Molecular Biology department. Christoph Bauer for his contributions to the cryoEM facility in Geneva (cryoGEnic). We also thank Orsolya Barabas for critical input and the Metabolomics Core Facility at EMBL Heidelberg for their Mass Spectrometry analysis. We acknowledge Diamond for access and support of the cryoEM facilities at the UK national electron bio-imaging centre (eBIC), proposal EM13708, funded by the Wellcome Trust, MRC and BBSRC. This work was supported by the Swiss National Science Foundation (310030_185235), the Schmidheiny, a Novartis Research grant (all awarded to A.B.), a grant from the U.S. National Institute of General Medical Sciences (R35-GM118053) to D.O.M., and an MRC grant (MC_UP_1201/6) to D.B.

References

1. Gruber S, Haering CH & Nasmyth K Chromosomal cohesin forms a ring. Cell 112, 765–77 (2003). [PubMed: 12654244]

2. Uhlmann F, Wernic D, Poupart MA, Koonin EV & Nasmyth K Cleavage of cohesin by the CD clan protease separin triggers anaphase in yeast. Cell 103, 375–386 (2000). [PubMed: 11081625]
3. Hauf S, Waizenegger IC & Peters JM Cohesin cleavage by separase required for anaphase and cytokinesis in human cells. Science 293, 1320–1323 (2001). [PubMed: 11509732]
4. Waizenegger IC, Hauf S, Meinke A & Peters JM Two distinct pathways remove mammalian cohesin from chromosome arms in prophase and from centromeres in anaphase. Cell 103, 399–410 (2000). [PubMed: 11081627]
5. Ciosk Ret al.An ESP1/PDS1 complex regulates loss of sister chromatid cohesion at the metaphase to anaphase transition in yeast. Cell93, 1067–1076 (1998). [PubMed: 9635435]
6. Stemmann O, Zou H, Gerber SA, Gygi SP & Kirschner MW Dual inhibition of sister chromatid separation at metaphase. Cell 107, 715–726 (2001). [PubMed: 11747808]
7. Boland Aet al.Cryo-EM structure of a metazoan separase-securin complex at near-atomic resolution. Nat. Struct. Mol. Biol24, 414–418 (2017). [PubMed: 28263324]
8. Luo S & Tong L Molecular mechanism for the regulation of yeast separase by securin. Nature 542, 255–259 (2017). [PubMed: 28146474]
9. Gorr IHet al.Essential CDK1-inhibitory role for separase during meiosis I in vertebrate oocytes. Nat. Cell Biol8, 1035–1037 (2006). [PubMed: 16906143]
10. Gorr IH, Boos D & Stemmann O Mutual inhibition of separase and Cdk1 by two-step complex formation. Mol. Cell 19, 135–41 (2005). [PubMed: 15989971]
11. Santaguida S & Amon A Short- and long-term effects of chromosome mis-segregation and aneuploidy. Nat. Rev. Mol. Cell Biol 16, 473–85 (2015). [PubMed: 26204159]
12. Kamenz J & Hauf S Time To Split Up: Dynamics of Chromosome Separation. Trends Cell Biol 27, 42–54 (2017). [PubMed: 27567180]
13. Rosen LEet al.Cohesin cleavage by separase is enhanced by a substrate motif distinct from the cleavage site. Nat. Commun10, 5189 (2019). [PubMed: 31729382]
14. Zou H, McGarry TJ, Bernal T & Kirschner MW Identification of a vertebrate sister-chromatid separation inhibitor involved in transformation and tumorigenesis. Science 285, 418–22 (1999). [PubMed: 10411507]
15. Li J, Ouyang YC, Zhang CH, Qian WP & Sun QY The cyclin B2/CDK1 complex inhibits separase activity in mouse oocyte meiosis I. Dev 146, dev182519 (2019).
16. Hellmuth S, Gómez-H L, Pendás AM & Stemmann O Securin-independent regulation of separase by checkpoint-induced shugoshin–MAD2. Nature 580, 536–541 (2020). [PubMed: 32322060]
17. Hellmuth Set al.Human chromosome segregation involves multi-layered regulation of separase by the peptidyl-prolyl-isomerase Pin 1. Mol. Cell58, 495–506 (2015). [PubMed: 25921067]
18. Shindo N, Kumada K & Hirota T Separase Sensor Reveals Dual Roles for Separase Coordinating Cohesin Cleavage and Cdk1 Inhibition. Dev. Cell 23, 112–23 (2012). [PubMed: 22814604]
19. Lin Z, Luo X & Yu H Structural basis of cohesin cleavage by separase. Nature 532, 131–4 (2016). [PubMed: 27027290]
20. Sullivan M, Hornig NCD, Porstmann T & Uhlmann F Studies on Substrate Recognition by the Budding Yeast Separase. J. Biol. Chem 279, 1191–6 (2004). [PubMed: 14585836]
21. Nagao K & Yanagida M Securin can have a separase cleavage site by substitution mutations in the domain required for stabilization and inhibition of separase. Genes to Cells 11, 247–60 (2006). [PubMed: 16483313]
22. Alexandru G, Uhlmann F, Mechtler K, Poupart MA & Nasmyth K Phosphorylation of the cohesin subunit Scc1 by Polo/Cdc5 kinase regulates sister chromatid separation in yeast. Cell 105, 459–72 (2001). [PubMed: 11371343]
23. Boos D, Kuffer C, Lenobel R, Körner R & Stemmann O Phosphorylation-dependent binding of cyclin B1 to a Cdc6-like domain of human separase. J. Biol. Chem 283, 816–23 (2008). [PubMed: 17974570]
24. Kõivomägi Met al.Multisite phosphorylation networks as signal processors for Cdk1. Nat. Struct. Mol. Biol20, 1415–1424 (2013). [PubMed: 24186061]
25. McGrath DAet al.Cks confers specificity to phosphorylation-dependent CDK signaling pathways. Nat. Struct. Mol. Biol20, 1407–14 (2013). [PubMed: 24186063]

26. Holland AJ, Böttger F, Stemmann O & Taylor SS Protein phosphatase 2A and separase form a complex regulated by separase autocleavage. J. Biol. Chem 282, 24623–32 (2007). [PubMed: 17604273]
27. Zou H, Stemman O, Anderson JS, Mann M & Kirschner MW Anaphase specific auto-cleavage of separase. FEBS Lett. 528, 246–50 (2002). [PubMed: 12297314]
28. Luo S & Tong L Structure and Function of the Separase-Securin Complex. in Harris JR, Marles-Wright J. (eds) Macromolecular Protein Complexes III: Structure and Function. 217–232 (Springer, Cham, 2021). doi:10.1007/978-3-030-58971-4_4
29. Bachmann Get al.A closed conformation of the Caenorhabditis elegans separase-securin complex. Open Biol. 6, 160032 (2016). [PubMed: 27249343]
30. Dephoure Net al.A quantitative atlas of mitotic phosphorylation. Proc. Natl. Acad. Sci. U. S. A105, 10762–7 (2008). [PubMed: 18669648]
31. Russo AA, Jeffrey PD, Patten AK, Massagué J & Pavletich NP Crystal structure of the p27(Kip1) cyclin-dependent-kinase inhibitor bound to the cyclin A-Cdk2 complex. Nature 382, 325–31 (1996). [PubMed: 8684460]
32. Cheng KYet al.The role of the phospho-CDK2/cyclin A recruitment site in substrate recognition. J. Biol. Chem281, 23167–79 (2006). [PubMed: 16707497]
33. Melesse M, Bembenek JN & Zhulin IB Conservation of the separase regulatory domain. Biol. Direct 13, (2018).
34. Goda T, Ishii T, Nakajo N, Sagata N & Kobayashi H The RRASK Motif in Xenopus Cyclin B2 Is Required for the Substrate Recognition of Cdc25C by the Cyclin B-Cdc2 Complex*. J. Biol. Chem 278, 19032–19037 (2003). [PubMed: 12754270]

Methods References

35. Zhang Z, Yang J & Barford D Recombinant expression and reconstitution of multiprotein complexes by the USER cloning method in the insect cell-baculovirus expression system. Methods 95, 13–25 (2016). [PubMed: 26454197]
36. Zhang Set al.Molecular mechanism of APC/C activation by mitotic phosphorylation. Nature533, 260–264 (2016). [PubMed: 27120157]
37. Martin TG, Boland A, Fitzpatrick AWP & Scheres SHW Graphene Oxide Grid Preparation. https://figshare.com/articles/Graphene_Oxide_Grid_Preparation/31786691 (2016). doi:10.6084/m9.figshare.3178669.v1
38. Stabrin Met al.TranSPHIRE: automated and feedback-optimized on-the-fly processing for cryo-EM. Nat. Commun11, 5716 (2020). [PubMed: 33177513]
39. Zheng SQet al.MotionCor2: Anisotropic correction of beam-induced motion for improved cryo-electron microscopy. Nat. Methods14, 331–332 (2017). [PubMed: 28250466]
40. Rohou A & Grigorieff N CTFFIND4: Fast and accurate defocus estimation from electron micrographs. J. Struct. Biol 192, 216–21 (2015). [PubMed: 26278980]
41. Wagner Tet al.SPHIRE-crYOLO is a fast and accurate fully automated particle picker for cryo-EM. Commun. Biol2, 218 (2019). [PubMed: 31240256]
42. Yang Z, Fang J, Chittuluru J, Asturias FJ & Penczek PA Iterative stable alignment and clustering of 2D transmission electron microscope images. Structure 20, 237–47 (2012). [PubMed: 22325773]
43. Wilkinson ME, Kumar A & Casañal A Methods for merging data sets in electron cryo-microscopy. Acta Crystallogr. Sect. D Struct. Biol 75, 782–791 (2019). [PubMed: 31478901]
44. Punjani A, Rubinstein JL, Fleet DJ & Brubaker MA CryoSPARC: Algorithms for rapid unsupervised cryo-EM structure determination. Nat. Methods 14, 290–296 (2017). [PubMed: 28165473]
45. Bepler Tet al.Positive-unlabeled convolutional neural networks for particle picking in cryo-electron micrographs. Nat. Methods16, 1153–1160 (2019). [PubMed: 31591578]
46. Zivanov J, Nakane T & Scheres SHW Estimation of high-order aberrations and anisotropic magnification from cryo-EM data sets in RELION-3.1. IUCrJ 7, 253–267 (2020).

47. Sanchez-Garcia Ret al.DeepEMhancer: A deep learning solution for cryo-EM volume post-processing. bioRxiv (2020). doi:10.1101/2020.06.12.148296

48. Kucukelbir A, Sigworth FJ & Tagare HD Quantifying the local resolution of cryo-EM density maps. Nat. Methods 11, 63–5 (2014). [PubMed: 24213166]

49. Adams PDet al.PHENIX: A comprehensive Python-based system for macromolecular structure solution. Acta Crystallogr. Sect. D Biol. Crystallogr66, 213–21 (2010). [PubMed: 20124702]

50. Emsley P, Lohkamp B, Scott WG & Cowtan K Features and development of Coot. Acta Crystallogr. Sect. D Biol. Crystallogr 66, 486–501 (2010). [PubMed: 20383002]

51. Brown NRet al.CDK1 structures reveal conserved and unique features of the essential cell cycle CDK. Nat. Commun6, 6769 (2015). [PubMed: 25864384]

52. Topf Met al.Protein Structure Fitting and Refinement Guided by Cryo-EM Density. Structure16, 295–307 (2008). [PubMed: 18275820]

53. Afonine PVet al.New tools for the analysis and validation of cryo-EM maps and atomic models. Acta Crystallogr. Sect. D Struct. Biol74, 814–840 (2018). [PubMed: 30198894]

54. Williams CJet al.MolProbity: More and better reference data for improved all-atom structure validation. Protein Sci27, 293–315 (2018). [PubMed: 29067766]

55. Yang Zet al.UCSF Chimera, MODELLER, and IMP: An integrated modeling system. J. Struct. Biol179, 269–78 (2012). [PubMed: 21963794]

56. Goddard TDet al.UCSF ChimeraX: Meeting modern challenges in visualization and analysis. Protein Sci. 27, 14–25 (2018). [PubMed: 28710774]

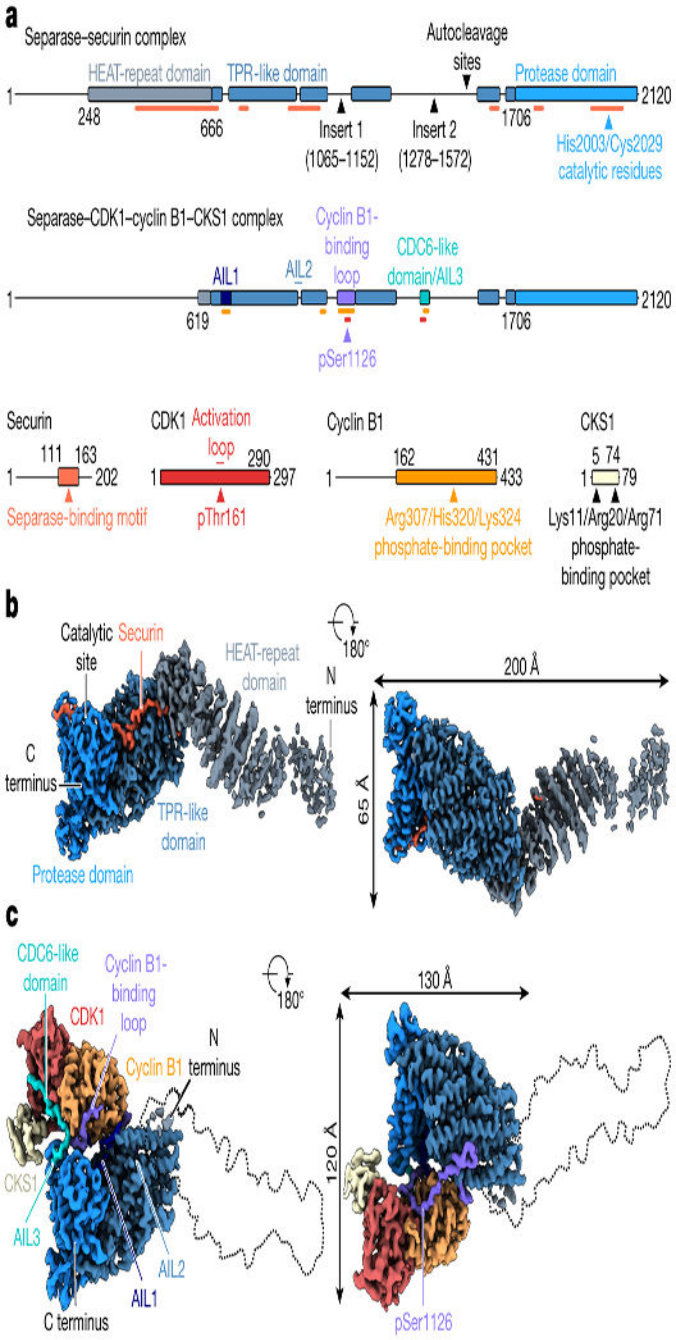

Fig. 1. Domain organization of *Homo sapiens* (*Hs*) separase-securin and separase-Cdk1-cyclin B1-Cks1 (CCC) complexes.

(**a**) Diagrams of the two complexes, with structured regions as blocks and undetected regions as solid lines. Insert 1 is disordered in separase-securin but is largely ordered upon CCC binding to become the cyclin B-binding loop. Three other disordered loops in separase-securin become ordered autoinhibitory loops (AIL1-3) in the CCC complex. Securin-binding sites on separase are indicated by orange lines in the top diagram. In the bottom diagram, red and yellow lines indicate Cdk1- and cyclin B1-binding sites on separase, respectively. (**b**,

c) Views of the cryoEM maps of the separase-securin (**b**) and separase-CCC (**c**) complexes, with each domain color-coded as in **a**.

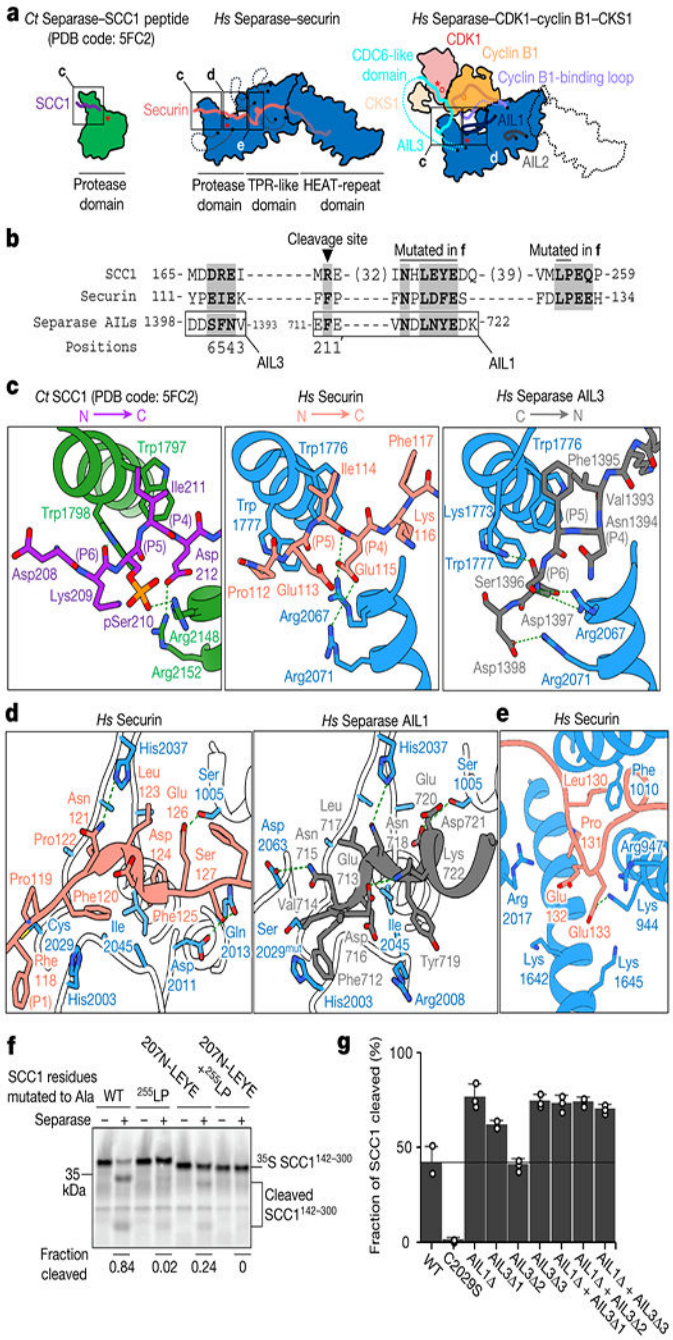

Fig. 2. Binding modes of an Scc1 peptide substrate, securin and the CCC complex to separase.

(a) Human (*Hs*) securin binds the length of separase. In the CCC complex, insert 1 and three autoinhibitory loops (AIL1-3) in separase become ordered and occupy binding sites on separase and Cdk1-cyclin B1, using conserved sequence motifs. For comparison, the protease domain of *C. thermophilum* (*Ct*) separase is shown at left. Red asterisks indicate active sites; red circles indicate phosphates. **(b)** Sequence alignment of EIExxΦ, NxLxΦE, and LPE motifs in human Scc1, securin, and separase. **(c)** Close-up of the binding interface between the Scc1 substrate-mimic (left), securin (middle) and AIL3 of separase (right) near

the catalytic site of separase. **(d)** Close-up view of the NxLxΦE binding motifs of securin and separase in the cleft adjacent to the separase active site. **(e)** Close-up view of the securin LPE motif bound to separase. **(f)** Separase-mediated cleavage of ^{35}S-labeled Scc1 mutants carrying alanine mutations in the NHLEYE motif and/or the LPE motif. Results are representative of four independent experiments. See also Extended Data Fig. 9. **(g)** Analysis of Scc1 cleavage by separase mutants with deletions in AIL1 and AIL3. Regions deleted in each mutant as follows (see Extended Data Table 2 for sequence details): AIL1Δ, deletion of AIL1, containing the NDLNYE motif; AIL3Δ1, deletion of Cdc6-like domain and NFS motif; AIL3Δ2, deletion of entire insert 2; AIL3Δ3, deletion of NFS motif. Results are representative of three independent experiments. Values represent mean +/− SEM (n=3). See also Extended Data Fig. 10a.

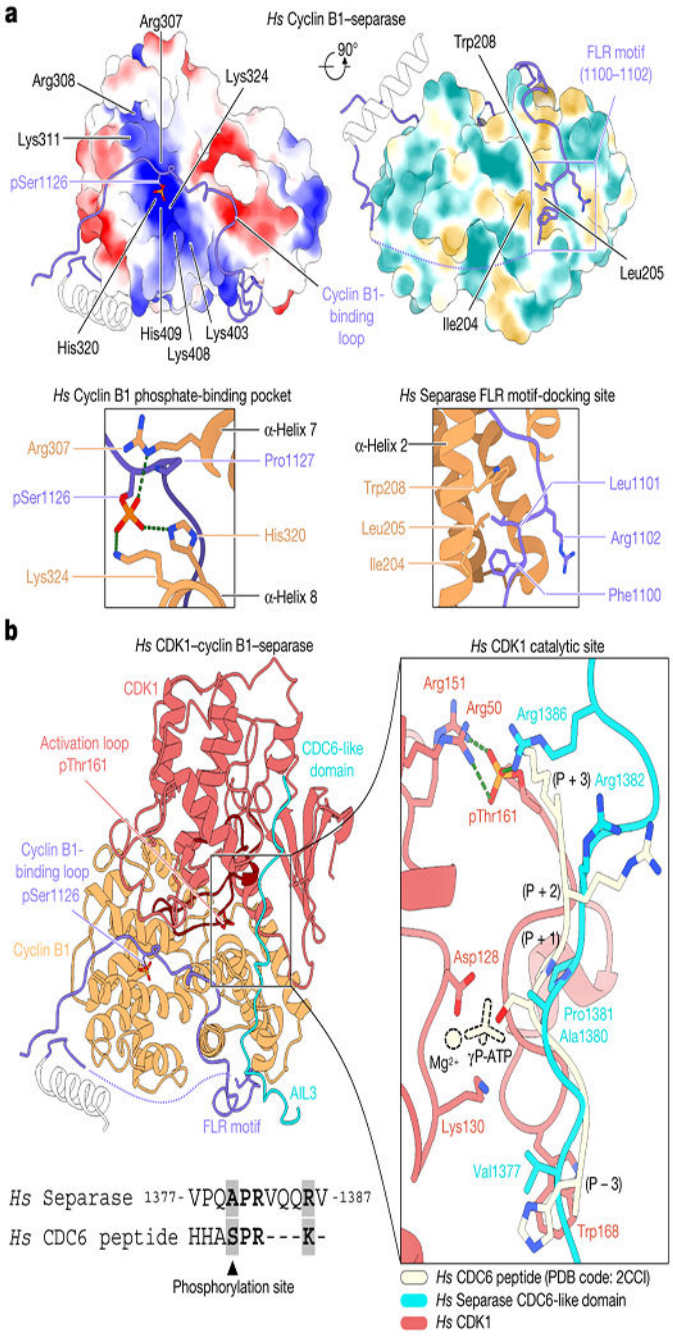

Fig. 3. Assembly of the separase-Cdk1-cyclin B1-Cks1 complex and structural basis for Cdk1 inhibition by separase.

(a) Two views of the surface of cyclin B1 (left) showing electrostatic potential and hydrophobicity, with close-ups of the key interactions at right. Electrostatic potentials are contoured from −10 (red) to +10 kT/e (blue). **(b)** Overview of separase interactions with Cdk1-cyclin B1. The cyclin B-binding loop and Cdc6-like domain of separase are shown in purple and cyan, respectively. Phosphothreonine 161 of Cdk1 and phosphoserine 1126 of separase are highlighted (left). At right is a close-up of Cdc6-like domain binding compared

to a substrate peptide (pale yellow) co-crystallized with Cdk2 (omitted) bound to ATP (PDB code: 2CCI[32]). The phosphoacceptor serine in the peptide substrate is replaced with Ala1380 of the Cdc6-like domain. Sequence conservation between the separase Cdc6-like domain and the substrate peptide is shown below.